

Semi-automated regional classification of the style of activity of slow rock-slope deformations using PS InSAR and SqueeSAR velocity data

Abstract Large slow rock-slope deformations, including deep-seated gravitational slope deformations and large landslides, are widespread in alpine environments. They develop over thousands of years by progressive failure, resulting in slow movements that impact infrastructures and can eventually evolve into catastrophic rockslides. A robust characterization of their style of activity is thus required in a risk management perspective. We combine an original inventory of slow rock-slope deformations with different PS-InSAR and SqueeSAR datasets to develop a novel, semi-automated approach to characterize and classify 208 slow rock-slope deformations in Lombardia (Italian Central Alps) based on their displacement rate, kinematics, heterogeneity and morphometric expression. Through a peak analysis of displacement rate distributions, we characterize the segmentation of mapped landslides and highlight the occurrence of nested sectors with differential activity and displacement rates. Combining 2D decomposition of InSAR velocity vectors and machine learning classification, we develop an automatic approach to characterize the kinematics of each landslide. Then, we sequentially combine principal component and K-medoids cluster analyses to identify groups of slow rock-slope deformations with consistent styles of activity. Our methodology is readily applicable to different landslide datasets and provides an objective and cost-effective support to land planning and the prioritization of local-scale studies aimed at granting safety and infrastructure integrity.

Keywords Slow rock-slope deformation · Deep-seated gravitational slope deformations · Landslide activity · Kinematics · InSAR · PS-InSAR · Multivariate statistical analysis

Introduction

Slow rock-slope deformations are common in mountain ranges worldwide. They affect entire hillslopes and displace volumes up to hundreds of millions of cubic meters (Bovis 1990; Chigira 1992; Saroli et al. 2005; Audemard et al. 2010; Agliardi et al. 2013; Crosta et al. 2013; Lin et al. 2013). Although characterized by very low displacement rates (mm/yr to cm/yr; Rott et al. 1999; Wasowski and Bovenga 2014; Frattini et al. 2018; Crippa et al. 2020), they damage infrastructures and may promote secondary failures. Heterogeneity and segmentation of these phenomena result in differential deformations of both surface (e.g. buildings, roads, pipelines) and underground structures (tunnels), strongly affecting the vulnerability of elements at risk with different structural characteristics, topologies and relative positions to different landslide sectors (Frattini et al. 2013).

The mechanism and internal segmentation of individual slow rock-slope deformations are constrained by inherited tectonic

features (Agliardi et al. 2001; Ambrosi and Crosta 2006; Agliardi et al. 2009; Stead and Wolter 2015) both at regional (e.g. major tectonic lineaments) and local scales (e.g. faults, folds, master fractures). In paraglacial environments, slow rock-slope deformations are promoted by stress and hydrological perturbations associated to deglaciation. These trigger progressive slope failure until the development of differentiated rockslides, sensitive to hydrological forcing and mirrored by complex creep behaviour (Crosta et al. 2013; Riva et al. 2018; Agliardi et al. 2020).

Slow rock-slope deformations are recognized by peculiar morpho-structural evidence (Zischinsky 1966; Radbruch-Hall et al. 1976; Massart 1983; Agliardi et al. 2001; Bovis 2013), including both extensional (double-crested ridges, trenches, scarps and counterscarps also associated in half-graben systems) and compressional features (toe bulging, thrusting and folding) that mirror deep deformation patterns and localization. These mass movements include a full spectrum of phenomena, ranging from deep-seated gravitational slope deformations (DSGSD) to large landslides (here LL). DSGSDs affect entire high-relief mountain slopes (>1000 m) involving the ridge crest and exhibit sharp morpho-structural features often controlled by inherited tectonic features. Large landslides are generally smaller than DSGSD (few square kilometres) and can evolve independently or nucleate within DSGSDs. In this case, large landslides show evidence of larger internal deformation and morphological maturity than the host DSGSD (Agliardi et al. 2012).

Because of the variability of their mechanisms, slow rock-slope deformations exhibit diverse styles of activity, defined by the interplay of displacement rate, kinematics and internal segmentation (Agliardi et al. 2012; Frattini et al. 2018). For example, landslides with translational global kinematics (Cruden and Varnes 1996; Hungr et al., 2014; Rainer et al., 2005; Rotaru et al., 2007) are intrinsically more unstable and prone to higher mobility than landslides with rotational kinematics. On the other hand, slope deformations characterized by similar kinematics and rates can evolve as coherent masses or break up in smaller sectors, depending on their structural segmentation and internal damage.

This complexity, associated with the low typical displacement rates, makes these phenomena difficult to tackle in a risk management perspective. Thus, a regional-scale classification is needed to gather a preliminary characterization of recognized phenomena.

Because of the depth and lack of characterization of basal shear zones, rarely reached by geotechnical and geophysical investigations (Brückl et al. 2006, 2013), the assessment of slow rock-slope deformation kinematics is not obvious and strongly relies on surface displacement measurements. In the past, these were limited to sparse traditional ground-based measurements (Bovis, 1990), unable to capture spatial displacements patterns. In the last

decades, spaceborne SAR radar interferometry (InSAR) became a powerful tool to characterize ground deformation rates from few millimetres to centimetres per year, acquiring information along the satellite line-of-sight (LOS; Gabriel et al. 1989). The technique maximizes the spatial and temporal coverage of wide areas and proved useful to map and assess the activity of landslides (Colesanti and Wasowski 2006; Del Soldato et al., 2019). In particular, multi-temporal persistent scatterer interferometry (PSI) techniques (e.g. PS-InSARTM, Ferretti et al. 2001; SqueeSARTM, Ferretti et al. 2011) allow measuring ground deformations with millimetric precision, making them suitable for regional-scale landslide mapping and inventory studies (Colesanti et al. 2003; Colesanti and Wasowski 2006; Rosi et al. 2014; Wasowski and Bovenga 2014; Frattini et al. 2018). However, as an intrinsic limitation of spaceborne SAR platforms, when true landslide deformation vectors deviate from the satellite line-of-sight (LOS), radar sensitivity decreases and slow movements become difficult to resolve (Schlögel et al. 2015; Eriksen et al. 2017; Crippa et al. 2020).

InSAR application to slow rock-slope deformations is further complicated by low signal-to-noise ratio and atmospheric and scatter (e.g. leaf) disturbances, limiting the number of PS, and by the ambiguities related to landslide mechanisms (Notti et al. 2012). Evaluating landslide activity in terms of mean along-slope projected velocity (Meisina et al. 2008; Notti et al. 2014; Tofani et al. 2014) is unsuitable for complex phenomena with kinematics unknown a priori. This can be better tackled using multi-geometry SAR processing combining ascending and descending data (2DInSAR; Eriksen et al. 2017).

In this paper, we use PSI products (TRE AltamiraTM), acquired over the alpine sector of the Lombardia region (Northern Italy; Fig. 1a), to propose a novel approach to characterize and classify slow rock-slope deformations based on their style of activity. We developed algorithms and Matlab/GIS tools that capture the kinematics, internal segmentation and activity of slow rock-slope deformations for a rapid regional-scale analysis. We use multivariate statistical analyses to achieve a robust style of activity classification of mapped slow rock-slope deformations and implement the procedures in a semi-automated workflow that can be readily applied to other landslide datasets in a fast and cost-effective way.

Study area

The study area (Fig. 1a) includes the alpine and prealpine sectors of Lombardia region. Here, N-verging Austroalpine and Penninic units are separated from the S-verging Southalpine units by the Insubric Line, a steep E-W trending fault zone active during Oligo-Miocene (Schmid 2017). Penninic units include oceanic lithosphere remnants (e.g. Malenco-Forno units) and portions of European margin (e.g. Adula, Tambò and Suretta nappe) and outcrop in western Lombardia (Valchiavenna and Valmalenco; Fig. 1a). Overlying Austroalpine units mainly consist of continental lithosphere of the Apulian margin, including metamorphic basement, intrusives and Mesozoic sedimentary successions (Florineth and Froitzheim 1994; Schmid 2017). They extend from Valmalenco to the eastern part of Valtellina (Fig. 1a) and are intruded by two major Tertiary tonalitic and granodioritic bodies outcropping in Valchiavenna-Val Masino (Masino-Bregaglia) and Val Camonica (Adamello). Southalpine units, south of the Insubric Line, form a fold-and-thrust belt made, from N to S, of a Variscan metamorphic

basement, Permian volcanoclastic and sedimentary successions and Mesozoic sedimentary succession including carbonate and terrigenous rocks (Fig. 1a).

The alpine sector is characterized by high peaks (up to 4000 m a.s.l.), high local relief and relatively steep topography, all progressively decreasing moving south towards the Southalpine sector and the foothills (Agliardi et al. 2013). This bulk topography is the result of complex interplay between rock type, Cenozoic tectonic forcing and Quaternary exhumation in fluvial and glacial environments (Sternai et al. 2012). During the Last Glacial Maximum (LGM; Ivy-Ochs et al. 2008; Grämiger et al. 2017), a thick ice cap covered the axial alpine sector with ice stages reaching 2800 m a.s.l. (Bini et al. 2009), feeding major valley glaciers (e.g. Adda and Oglio) that carved the topography reaching the Po Plain to the south. Post-LGM deglaciation caused major stress and hydrological perturbations that triggered paraglacial slope response and progressive failure (Grämiger et al. 2017; Riva et al. 2018; Spreafico et al. 2020). Fluvial incision reshaped the valleys especially in the prealpine and foothill areas. These perturbations promoted the onset and spatial distribution of large, slow rock-slope deformation (Ambrosi and Crosta 2006; Agliardi et al. 2013; Pánek et al. 2019), modulated by lithology and preconditioned by inherited tectonic structure on different scales, from clustering around regional tectonic boundaries (Agliardi et al., 2013) to slope scale controls by master fractures and folds (Agliardi et al., 2001, 2009, 2019a, b; Pedrazzini et al., 2016). Slow rock-slope deformations are widespread in axial alpine areas characterized by medium-strength anisotropic (e.g. foliated) rocks, high local relief and valley incision and tend to cluster along major tectonic structures. In areas with sedimentary rocks and relatively low relief (e.g. Southern Alps), giant slow rock-slope deformations are less frequent and often controlled by second-order stratigraphic and structural features (Crosta and Zanchi 2000; Agliardi et al. 2013) that can only be accounted for in site-specific studies.

Materials and methods

A robust characterization of the style of activity of slow rock-slope deformations must consider the interplay between their displacement rates, kinematics and complexity (e.g. segmentation, heterogeneity, internal damage, structural controls). To this aim, we combine an original geomorphological mapping dataset with different PS-InSARTM and SqueeSARTM datasets to develop a novel approach to characterize and classify slow rock-slope deformations on a regional scale using deterministic and multivariate statistical analyses.

Geomorphological mapping

We consider 208 slow rock-slope deformations selected from different inventories (GeoIFFI landslide inventory, Ceriani and Fossati 2005; DSGSD inventory, Crosta et al. 2013, Agliardi et al. 2013), including 134 deep-seated gravitational slope deformations (DSGSDs) and 74 large landslides. The latter are extracted from the GeoIFFI database based on areal extent (area >1.5 km², >1 km² when interacting with elements at risk) and practical relevance (e.g. actively monitored or undergoing remediation works).

Selected slow rock-slope deformations cluster in alpine sectors (e.g. Val Chiavenna, Valtellina, upper Orobic Alps; Fig. 1). Some have already been studied in detail (Crosta 1996; Crosta and

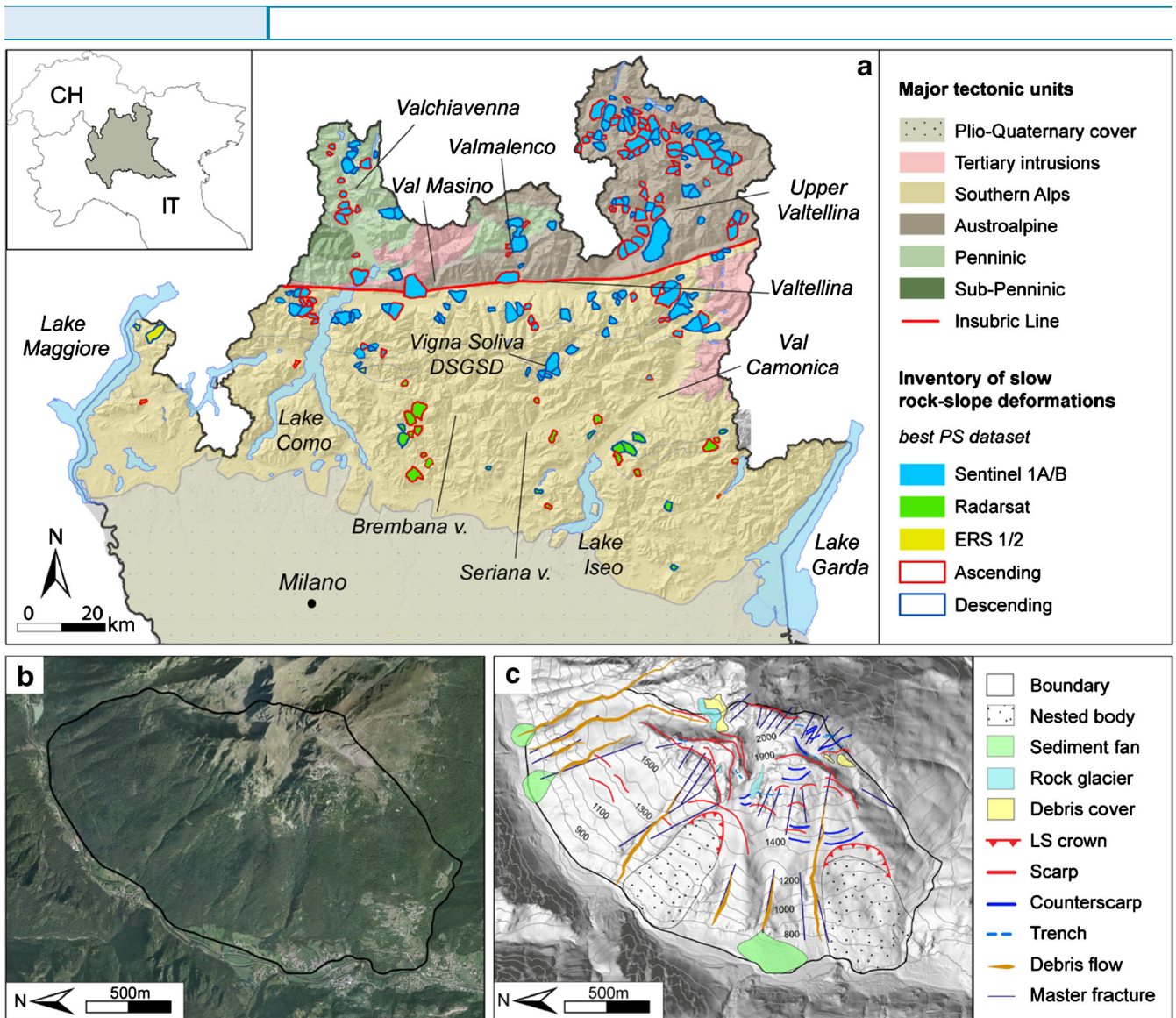


Fig. 1 Inventory of slow rock-slope deformations in Lombardy region and relative mapped features. (a) 208 slow rock-slope deformations, classified by the InSAR dataset selected for the analysis and best satellite acquisition geometry. Major tectonic units (Schmid et al. 2004) are reported. Mapping example: Vigna Soliva DSGSD, (b) orthophoto and (c) geomorphological map

Zanchi 2000; Agliardi et al. 2001; Zanchi et al. 2002; Allievi et al. 2003; Ambrosi and Crosta 2006; Agliardi et al. 2009), also with the support of PSInSAR™ data (Ambrosi and Crosta 2006; Frattini et al. 2018).

We perform an original geomorphological mapping of the selected cases by detailed photo-interpretation of aerial stereophotos (Regione Lombardia TEM1 series, 1981-1983; nominal scale 1:20000), digital orthophotos (2000; resolution 1m, 2007, 2012, 2015; resolution 0.5m), GoogleEarth™ imagery and Digital Elevation Models (Regione Lombardia, cell size: 5m), validated by local field visits and literature data. Our geomorphological dataset includes major slope-scale features, allowing a rapid mapping of hundreds of cases yet providing site-specific information to support the evaluation of geometry, kinematics, accumulated deformation and long-term activity. The dataset includes six vector layers, namely (Figs.

1b,c): (1) landslide boundaries (polygons), (2) nested landslides (immature or deformed, polygons), (3) areal geomorphological features (polygons, e.g. debris fans, shallow landslide deposits, sediment fans, periglacial features), (4) linear geomorphological features (polylines, e.g. debris flow channels, erosion gullies), (5) gravitational morpho-structures (polylines, e.g. scarps, counterscarps, trenches) and (6) tectonic lineaments (polylines).

For each mapped case, we extract the dominant lithology from a published 1:250,000 digital geological map (Montrasio et al. 1990). Lithostratigraphic units are grouped into 9 rock type classes (Table 1) based on their typical geomechanical behaviour (Agliardi et al. 2013), namely: carbonates (C), foliated metamorphics (MF), massive metamorphics (M), clastic rocks (S), quartzite (Q), orthogneiss (OT), flysch-type rocks (FL), granitoid/metabasite (IT) and volcanic rocks (V).

We also consider a set of morphometric variables (Lebuis et al. 1983; Hengl and Reuter 2008; Mansour et al. 2015; Table 1), namely: (1) elongation ratio (L/W), (2) shape factor (A/2p), (3) relief (Δh), (4) mean aspect (aspect), (5) mean slope angle (slope) and (6) hypsometric integral (Hi). Moreover, we include the following geomorphological variables as proxies of the mechanisms, damage state and long-term evolution of slow rock-slope deformation (Table 1): (1) immature

nested landslide density (NB), (2) deformed nested landslide density (DB), (3) landslide scarp sector density (LS) and (4) morpho-structure density (DM).

InSAR data

We use 3 different PS-InSARTM and SqueeSARTM datasets (TRE AltamiraTM) derived from ERS 1-2, Radarsat and Sentinel 1A/B C-band SAR imagery. Images were acquired between 1992 and 2017

Table 1 Lithological, morpho-structural, morphometric and InSAR-derived variables, quantified for each of the 208 slow rock-slope deformations and considered for multivariate statistical analysis

Rock type	Description	
C	Carbonate rocks (both massive and layered)	
S	Sedimentary clastic rocks	
FL	Flysch-type rocks	
M	Massive metamorphic rocks	
MF	Phyllosilicate-rich foliated metamorphic rocks	
OT	Quartz-rich foliated metamorphic rocks	
IT	Intrusive rocks	
Q	Quartzite	
Morpho-structure	Definition	Description
Density of immature nested landslide (NB)	(Nested area/total landslide area)*100	Areal density of nested bodies in an embryonic stage of evolution
Density of deformed nested landslide (DB)	(Nested area/total landslide area)*100	Areal density of nested bodies in an advanced stage of evolution
Landslide scarps (LS)	(Scarp area/total landslide area)*100	Proxy of total accumulated landslide strain
Density of linear morpho-structures (DM)	Total morpho-structure length/landslide area	Proxy of internal damage
Morphometry	Definition	Description
Elongation ratio (L/W)	Landslide length (L)/width (W)	Form factor assuming an elliptical landslide area with axes L and W
Shape factor (A/2p)	Landslide area (A)/landslide perimeter (2p)	Form factor based on the ratio of landslide spatial and linear extent
Relief (Δh)	$\Delta h = \text{maximum elevation} - \text{minimum elevation}$	Relief energy in the landslide area
Hypsometric integral (Hi)	$Hi = \frac{\text{Mean elevation} - \text{minimum elevation}}{\text{Maximum elevation} - \text{minimum elevation}}$	Proxy of the morphological maturity of the landslide area
Mean aspect	Mean azimuth (dip direction) of the landslide area	Mean aspect calculated as circular mean of each pixel
Activity (InSAR)	Definition	Description
Modal LOS velocity (v_PM)	Most frequent peak velocity	Modal landslide LOS velocity (mm/yr), equal to the highest velocity frequency peak (Fig. 7)
Velocity of the smallest peak (v_Pm)	Less frequent peak velocity	Velocity corresponding to the smallest velocity frequency peak identified
Quartile deviation (Q_dev)	$Q_{Dev} = \frac{Q_3 - Q_1}{Q_3 + Q_1}$	Dispersion of the velocity frequency distribution in each landslide, proxy of velocity heterogeneity
Δ Skewness(Δ_{SK})	Skewness of Δ distribution	Asymmetry of the frequency distribution curve of Δ angles (Fig. 4)
Δ Median(Δ_M)	Median of Δ distribution	Median value of Δ angle frequency distribution (Fig. 4)

Table 2 InSAR PSI datasets used in the analysis

Satellite	PSI technique	Mode	Θ (°)	Δ (°)	Revisit time (days)	Time interval (years)
ERS 1/2	PSInSAR TM	Ascending	23.20	~13.00	35	1992–2003
ERS 1/2	PSInSAR TM	Descending	23.09	~12.00		1992–2000
RADARSAT-S3	SqueeSAR TM	Ascending	32.49	12.12	24	2003–2007
RADARSAT-S3	SqueeSAR TM	Descending	36.27	9.60		2003–2007
Sentinel 1A/B	SqueeSAR TM	Ascending	41.99	10.23	12	2015–2017
Sentinel 1A/B	SqueeSAR TM	Descending	41.78	8.89	(6 after 2016)	2015–2017

along ascending and descending tracks (Table 2) and processed over the entire study area.

For each mapped rock-slope deformation (Fig. 1a), we select a reference best dataset, characterized by the highest spatial density of PS (permanent scatterers) and DS (distributed scatterers) and the most suitable acquisition geometry. The latter is selected depending on landslide slope and aspect parameters (Figs. 2a,b) and satellite orbit parameters (LOS and azimuth angle), according to the C index (Notti et al., 2012, 2014; Fig. 2c). This index quantifies the amount of along-slope movement that can be recorded by a SAR sensor with specific orbital and LOS directions. Datasets derived from Sentinel 1A/B images always provide the best spatial coverage and highest number of PS and DS and, when available, are preferred in the analysis. Since velocity values associated to PS and DS data can be locally related to shallow movements of slope deposits (e.g. scree, periglacial features) and not directly related to deep-seated landslides (Meisina et al. 2008; Frattini et al. 2018), we remove PS inside slope deposits. To this aim, we use geomorphological maps accompanying the GeoIFFI inventory, refined by interpretation of Google EarthTM imagery and recent orthophotos.

The robustness of InSAR data analyses is affected by the density and distribution of active PS or DS within individual landslides (Frattini et al. 2018; online Resource Fig.S1), which depend on slope orientation (aspect and inclination) and vegetation cover. Fewer PS and DS limit the statistical robustness of velocity value samples, resulting in a more uncertain definition of landslide segmentation, representative velocities and kinematics. As a

limiting condition, less than three PS or pseudo-PS hamper the spatial interpolation of LOS velocity, required to retrieve information on landslide segmentation, degree of activity and kinematics.

Deterministic analysis: segmentation, heterogeneity and kinematics

The simplest InSAR-based descriptor of landslide activity is the mean LOS velocity of active scatterers inside each landslide area. We consider “active” all the PS and DS with coherence > 0.7 and associated mean velocity outside the non-specific uncertainty (noise) range of ± 2 mm/yr, commonly used in regional-scale studies (Bianchini et al., 2015; Del Ventisette et al., 2015; Raspini et al., 2018; Ciampalini et al., 2019). However, the mean LOS velocity computed from point-like PS and DS over a landslide area may not represent its actual activity (Frattini et al. 2018). In fact, large slope deformations are often characterized by nested sectors faster than the main body, as well as heterogeneities related to rock mass damage and active morpho-structures (Crippa et al. 2020), resulting in large LOS velocity variability.

We thus develop an objective method to characterize the internal segmentation of each landslide, based on the identification of peaks on the frequency distribution curve of LOS velocity (Fig. 3). In general, landslide bodies with little internal damage or segmentation (Fig. 3a) exhibit homogeneous displacement fields and unimodal velocity distributions (Fig. 3b). On opposite, landslides with segmented activity (Fig. 3c) are characterized by multimodal velocity distributions (Fig. 3d).

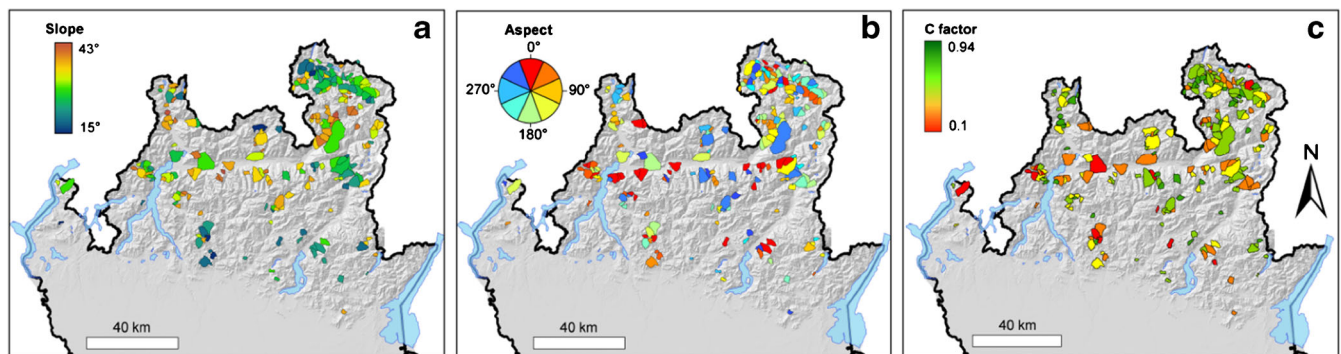


Fig. 2 Maps of mean slope (a), aspect (b) and C factor (c) computed on each landslide. C values (Notti et al., 2012, 2014) indicate the amount of along-slope movement that can be recorded by a SAR sensor on each slope according to its morphometry and orbital parameters. High values of C correspond to favorably oriented slopes (green in the map) that are better sensed by the satellites, low values point out landslides with unfavorable orientation (red values)

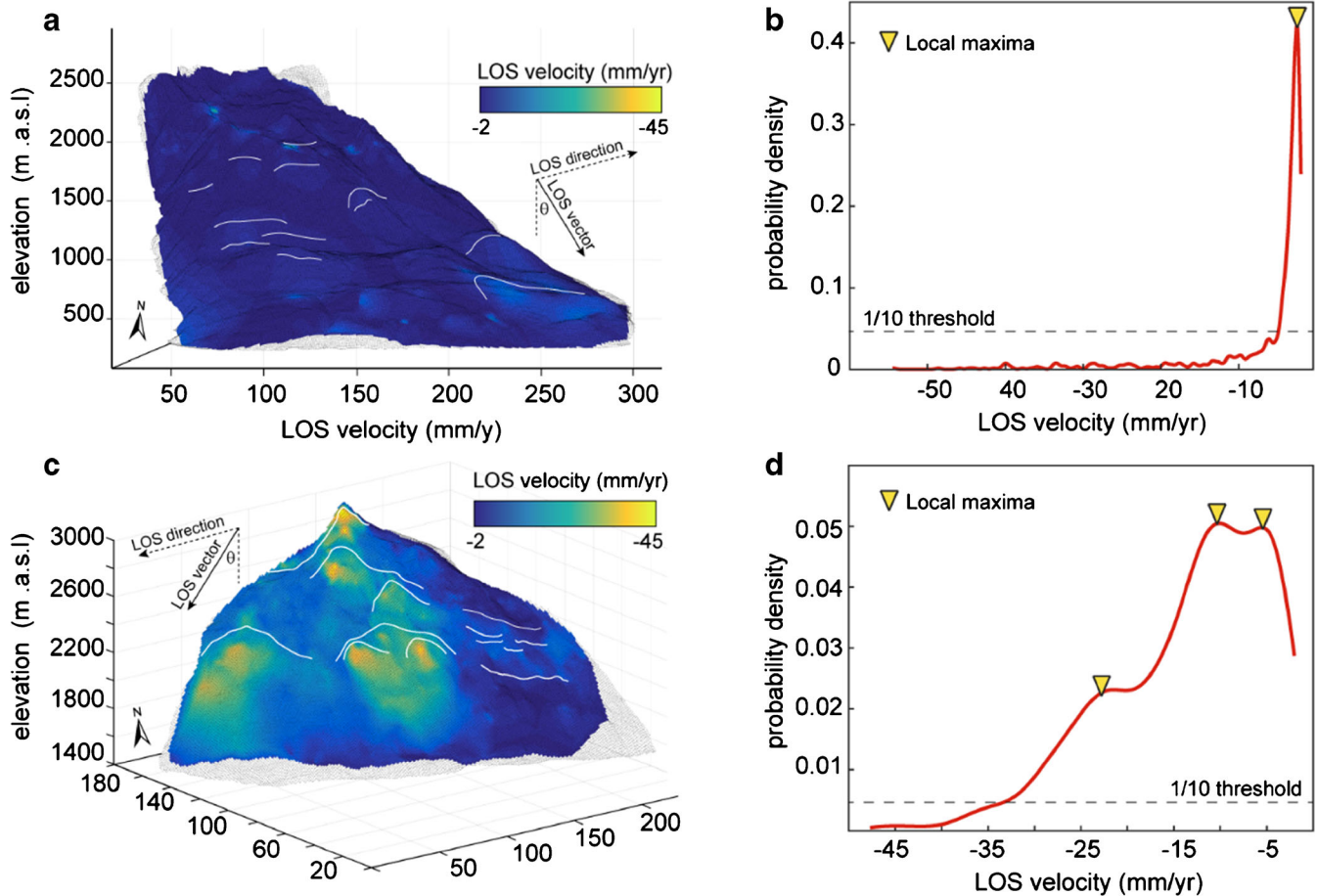


Fig. 3 Products of the segmentation analysis. (a) homogenous DSGSD with a constant velocity field over the entire slope. (b) Probability density curve showing a single peak value corresponding to the most frequent velocity value. (c) Example of a segmented DSGSD with slope sectors characterized by different displacement rates. (d) Corresponding density curve with several peaks indicating a heterogeneous displacement field. Peaks are identified as local maxima in the curve exceeding an arbitrary threshold

In our analysis, peaks are defined as local maxima exceeding a certain probability density threshold that can be set arbitrarily to detect peaks with different relevance. In this study, we set its value to 1/10 of the maximum probability density. Each detected peak represents the distribution of a specific cluster of velocity values, without providing clues on its spatial distribution. Distinct peaks emerging from the threshold indicate the occurrence of clearly segmented domains, each characterized by a given mean velocity and dispersion. Minor peaks (frequency < threshold) are usually related to outliers or noise. We quantify the activity heterogeneity (i.e. dispersion of velocity values) of each landslide in terms of quartile deviation $Q_Dev = (Q_3 - Q_1) / (Q_3 + Q_1)$, where Q_1 and Q_3 are the 25th and 75th percentiles of the velocity distribution, respectively. Larger heterogeneity is mirrored by a larger value of Q_Dev .

Slope deformation kinematics can be estimated using a multi-geometry analysis of InSAR data, combining measurements provided by ascending and descending tracks to decompose the 2D velocity vector in the E-W trending vertical plane (2D-InSAR; Dalla Via et al. 2012; Eriksen et al. 2017; Crippa et al. 2020). We developed a MatlabTM script to automatically discretize each landslide area into regular square cells (size: 25 m), in which the

average LOS velocity of PS and DS from the same acquisition geometry is assigned to cell centroids. For each “pseudo-PS” (i.e. cell centroids for which information from both ascending and descending data are available), the script derives the vertical (V_v) and horizontal (V_e) displacement rate components, the 2D displacement rate vector V_T in the E-W vertical plane, as well as its inclination τ (Manzo et al. 2006; Dalla Via et al. 2012; Eriksen et al. 2017; Crippa et al. 2020). The cell size (25 m) was selected to optimize the number of pseudo-PS and the accuracy of computed mean velocity values, avoiding mixing distant scatterers. In slopes with spatially heterogeneous deformations, large cells (100 m) can extend over different deformation domains, resulting in unrealistic estimates of local kinematics. On the contrary, small grid cells (10 m, below the spatial resolution of the sensor, about 20 m for Sentinel-1) result in a reduced probability of finding pseudo-PS.

The local (cell-scale) slope kinematics can be readily inferred (Agliardi et al. 2019b) by observing the difference between the 2D velocity vector inclination (τ) and the local slope dip (α) in each square cell, namely $\Delta = \tau - \alpha$ (Fig. 4a). Where Δ is positive, we have a dominant downward movement dipping in the slope (Figs. 4b,c). Values of Δ close to zero indicate slope-parallel sliding, while

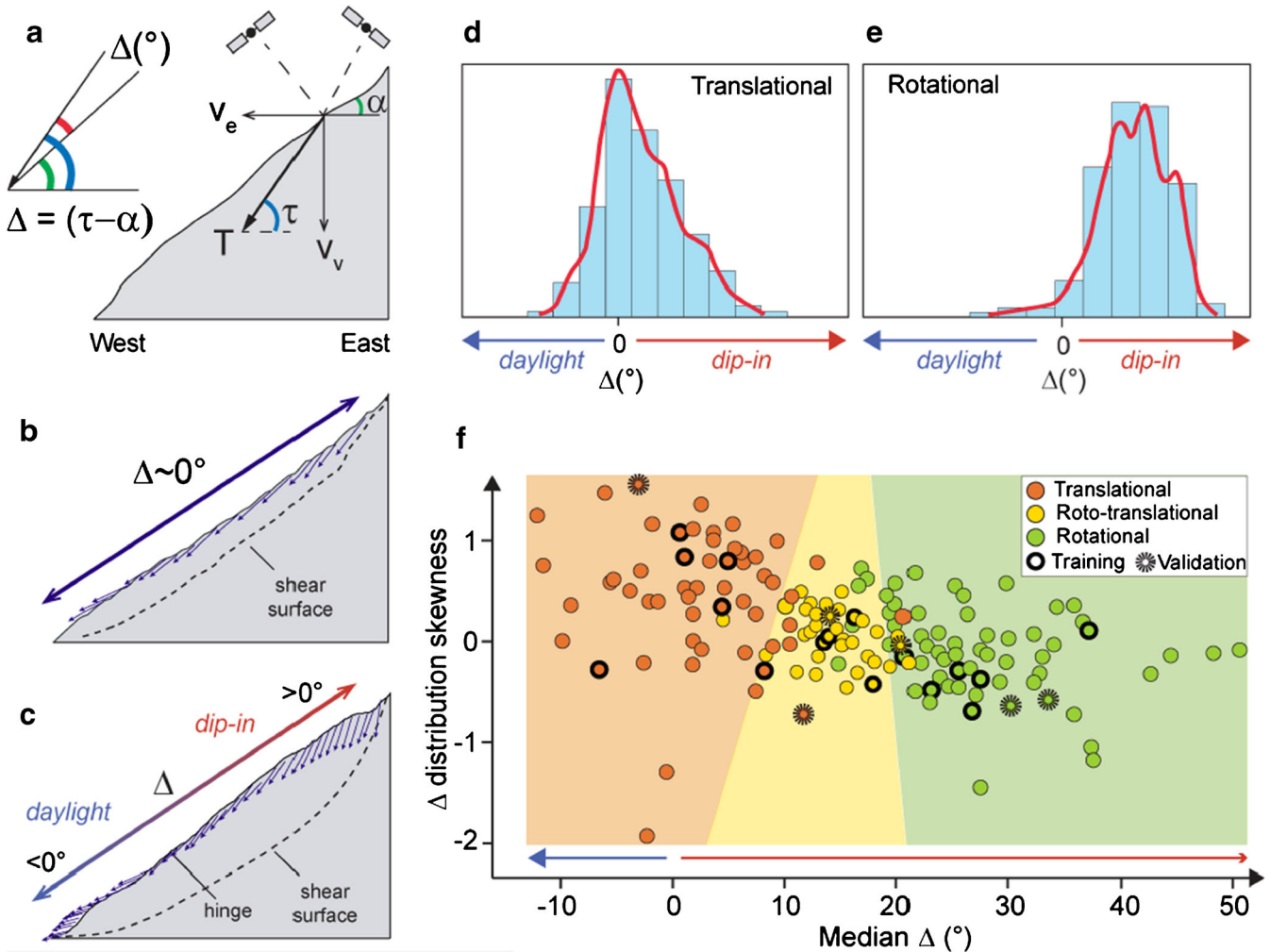


Fig. 4 Results of the kinematic analysis. (a) quantities considered in the analysis. α : local slope angle; τ : inclination of the 2D velocity vector derived by 2D SAR decomposition; Δ : difference between α and τ . Δ values distinguish (b) along slope movement and (c) dip-in or daylight displacements. Δ value distribution over a landslide area provides an indicator of its main deformation style: (d) translational; (e) rotational. (f) machine learning classification of mapped landslide kinematics according to Δ distribution skewness and median. The background coloured fields correspond to the kinematic groups (R, RT, T) and are defined using linear discriminant decision surfaces

negative values indicate daylighting or bulging movements. The global (i.e. slope-scale) landslide kinematic is inferred by analysing the statistical distribution of the parameter Δ within each entire landslide area (Figs. 4d,e). In particular, the frequency distribution of Δ values of translational landslides tends to be symmetrical and centred around zero or slightly shifted towards positive (“dip-in”) values, accounting for the local kinematics of scarp areas (Fig. 4d). Instead, rotational landslides have either bimodal distributions or distributions skewed towards positive values, as the displacement vector becomes steeper within the entire mass and daylight (negative Δ) at the toe (Figs. 4e).

In order to exploit this concept in a regional-scale analysis, we use Δ descriptive statistics (i.e. mean, mode, median, skewness, kurtosis) as inputs to a supervised machine learning analysis through the Matlab™ “classification learner” tool. This trains different classification models (e.g. decision trees, discriminant analysis, support vector machines, logistic regression, nearest neighbours, naïve Bayes

and ensemble classification) to select the best-performing ones. We train the model on a subset of 16 landslides (Online Resource Fig. S2) with known kinematics (Agliardi et al. 2001; Allievi et al. 2003; Ambrosi and Crosta 2006; Frattini et al. 2018) and generate predictions for the remaining data. Linear discriminant (Fisher, 1936) proves to be the best predictive model, with a mean accuracy higher than 80% over several (>20) iterations. We also validate the result using a subset of 6 selected case studies (Online Resource Fig. S2) and by local-scale detailed observation of morpho-structures, providing surface expression of the deep mechanisms. Our results show that the median (Δ_M) and in minor portion skewness (Δ_{SK}) of the frequency distribution of Δ values are effective predictors of global landslide kinematics (Fig. 4f).

Multivariate statistical analysis: PCA and cluster analysis

We run a series of multivariate statistical analyses, including principal component analysis (PCA, Pearson 1901; Hotelling 1933;

Ballabio 2015; Cohen-Waeber et al. 2018) and cluster analysis, to identify the lithological, morphometric, morpho-structural and InSAR-derived activity variables (Table 1 and Table 2) that influence the style of activity of slow rock-slope deformations at the regional scale for classification. After a careful evaluation of the activity of landslides with different dominant lithologies (Online Resource Fig. S1), we excluded this variable from the subsequent analyses. In fact, although rock type is a well-recognized control on the occurrence of slow rock-slope deformations (Agliardi et al. 2013; Crosta et al. 2013; Pedrazzini et al. 2016), on regional scale, it appears uncorrelated with activity and kinematics (Online Resource Fig. S3).

In the different analysis steps, we keep principal components with eigenvalues > 1 . Cases missing values of some variables, e.g. due to lack of PS, DS or pseudo-PS, are automatically excluded from the PCA according to a listwise deletion procedure.

We use PCA results as inputs for an unsupervised cluster analysis, aimed at detecting similarities and classifying cases into few groups (Massart 1983; Ballabio and Consonni 2013; Ballabio 2015), representative of different styles of activity. For the cluster analysis, we use the K-medoids method instead of the traditional K-means. K-medoids uses actual sample points as cluster centres (Kaufman and Rousseeuw 1990; Jin and Han 2010). Medoids are selected randomly from data objects to form n clusters, and remaining data objects are grouped to minimize the sum of dissimilarities of the surrounding points, making the approach more robust to noises and outliers (Arora and Varshney 2016).

We perform the following multivariate analyses (MV), i.e. PCA and cluster analysis, considering the following subsets of landslides and variables:

- **MV1:** rock-slope deformations (DSGSDs + large landslides) covered by InSAR data (166 cases out of 208), considering 14 variables: 5 morphometric, 4 morpho-structural and 5 InSAR-derived related to activity and kinematics (Table 1)
- **MV2:** all the mapped rock-slope deformations (DSGSDs + large landslides, 208 cases), considering 9 variables: 5 morphometric and 4 morpho-structural (no InSAR variables; Table 1)
- **MV3:** DSGSDs covered by InSAR data (117 cases), considering 14 variables: 5 morphometric, 4 morpho-structural and 5 InSAR-derived (Table 1)
- **MV4:** large landslides covered by InSAR data (49 cases), considering 14 variables: 5 morphometric, 4 morpho-structural and 5 InSAR-derived (Table 1)
- **MV5:** proximity analysis on rock-slope deformations (DSGSDs + large landslides) not covered by InSAR data (42 cases)

Results

Slow rock-slope deformation segmentation, activity and kinematics

Our results, validated using field data, show that 57 slow rock-slope deformations move as coherent blocks (“homogenous” class, e.g. Mt. Letè in Fig. 5a), while most mapped cases undergo a variable degree of internal segmentation. Segmented landslides are usually characterized by one (55 cases) or two (81 cases) distinct nested sectors, with different LOS velocity than the background, e.g. Mt. Padrio Varadega DSGSD (Ambrosi and Crosta

2006) and Mt. Mater (Crippa et al. 2020). Fifteen cases are very segmented, with more than three nested sectors (Fig. 5a; e.g. Corna Rossa DSGSD, Agliardi et al. 2018).

Modal values of LOS velocity representing the state of activity of main landslide bodies are generally in the range of 3–5 mm/yr (absolute values). When landslide movements are homogeneous, mean and modal velocities tend to converge. Mean landslide velocity (Fig. 5b) usually exceeds the modal one (Fig. 5c) when the main landslide body hosts smaller and faster nested sectors. On opposite, modal velocity exceeds the mean one (Fig. 5d) when faster nested sectors, with abundant PS and DS, involve a high percentage of the total landslide extent (e.g. Piz Groppera large landslide, Valchiavenna n°4 in Fig. 11). Differences between modal and mean velocity are usually in the range of few mm/yr, but can reach several mm/yr (e.g. Belviso n°12 in Fig. 11: mean velocity ~13 mm/yr, modal velocity ~15 mm/yr) and up to 1 cm (e.g. Piz Groppera: mean velocity ~33 mm/yr, modal velocity ~42 mm/yr).

Our objective quantification of landslide global kinematics allows classifying the mapped landslide population into translational, roto-translational and rotational landslides (Figs. 4 and Fig. 5e). Mapped slow rock-slope deformations have dominant rotational (72 cases) or roto-translational kinematics (42 cases), while 57 cases exhibit translational kinematics (Figs. 5e,f).

Style of activity classification

MV1: DSGSD and large landslides covered by InSAR data, all variables PCA on the bulk inventory (including both DSGSDs and large landslides) allows characterizing only 166 landslides out of 208. In fact, 42 cases with less than 3 active PS or lacking pseudo-PS are automatically discarded from PCA by listwise deletion.

In this analysis, we select the first 6 principal components (PCs), accounting for about 70% of the entire multivariate space variance, and focus on the relationships between the first three principal components (PC1, PC2 and PC3, Fig. 6), which explain about 49% of the variance.

PC1 and PC2 loadings (Fig. 6a) are mainly related to morphometric and morpho-structural variables. The strongest control on PC1 is exerted by the density of immature nested landslides (NB) and deformed nested landslides (DB), which distribution is complementary as suggested by their opposite direction along PC1. PC2 is mainly related to the hypsometric integral (Hi), the relief energy (Δh) and the density of morphostructures (DM). PC3 (Fig. 6b) accounts for InSAR-derived parameters such as modal LOS velocity (v_{PM}), quartile deviation (Q_{dev}) and kinematics statistics (Δ_{SK} , Δ_M).

The PC1/PC2 biplot (Fig. 6a) shows a clear trend along PC1, corresponding to different distributions of cases pre-classified as “DSGSD” and “large landslide” in the inventory. The distinction between the two classes is dominated by their morphological features, such as a different L/W (i.e. more elongated shape for large landslides), and the abundance of deformed nested bodies (DB) in large landslides with respect to DSGSDs, the latter hosting abundant immature nested bodies (NB). The same distinction between DSGSD and large landslide groups is evident in the PC1/PC3 plot (Fig. 6b). We checked the statistical consistency of the inventory pre-classification into these 2 classes by performing a K-medoids cluster analysis on the first 3 PCs (Fig. 6c,d), repeating the analysis 20 times to improve the robustness of the classification.

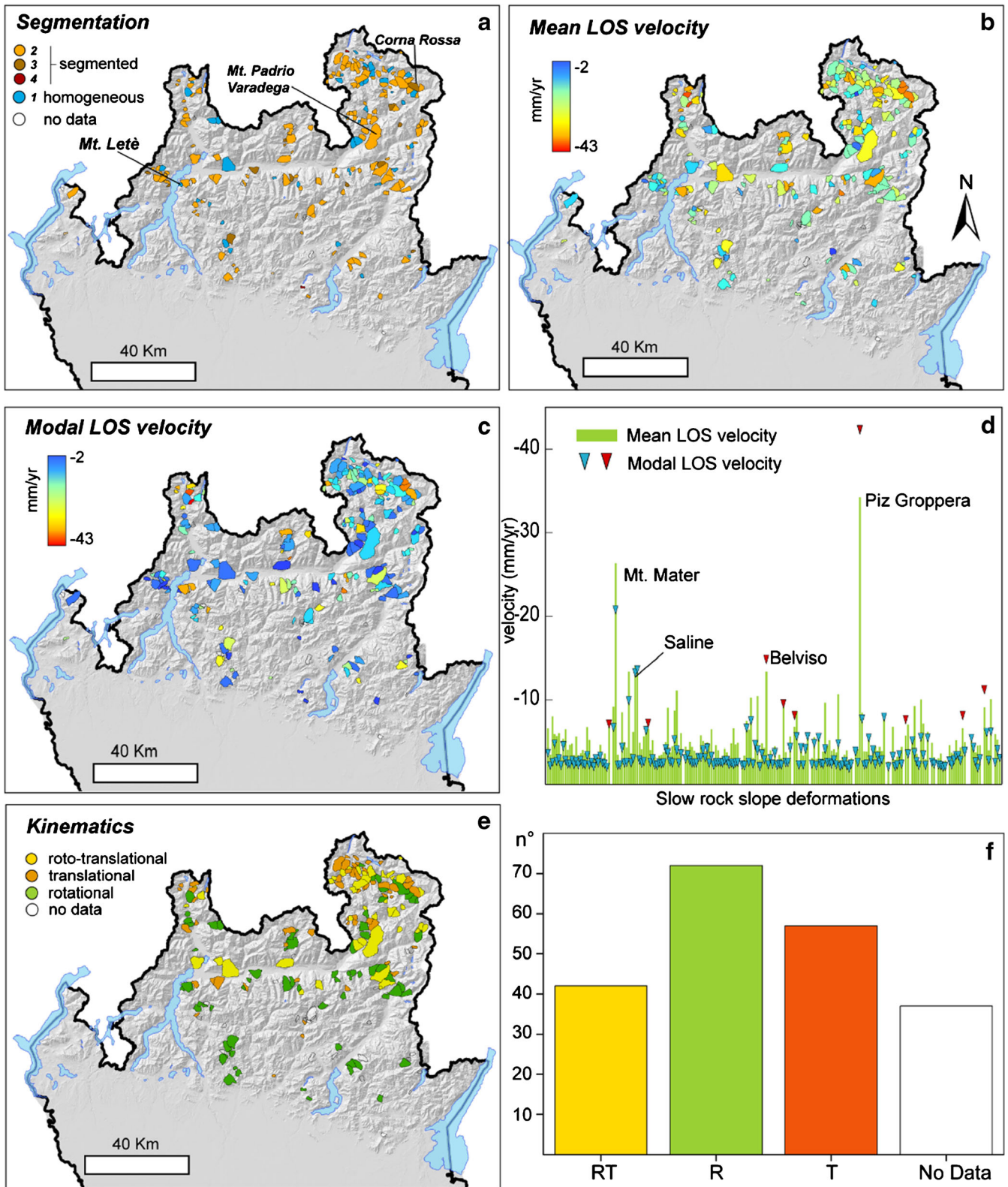


Fig. 5 Maps showing distribution of activity, segmentation and kinematics over the entire inventory. (a) Distribution of segmented and homogeneous phenomena with associated indicative number of internal sectors outlined by the peak analysis. (b) Mean LOS velocity computed for each landslide considering active PS (velocity < -2 mm/yr). (c) Modal LOS velocity resulting from the peak analysis on active PS distribution for each landslide. (d) plot representing the mean LOS velocity and the peak LOS velocity for each element. Red triangles correspond to some evident cases in which the peak velocity exceeds the mean value. (e) distribution of kinematics and (f) bar plot representing the frequency distribution of slow rock-slope deformations by type of kinematism

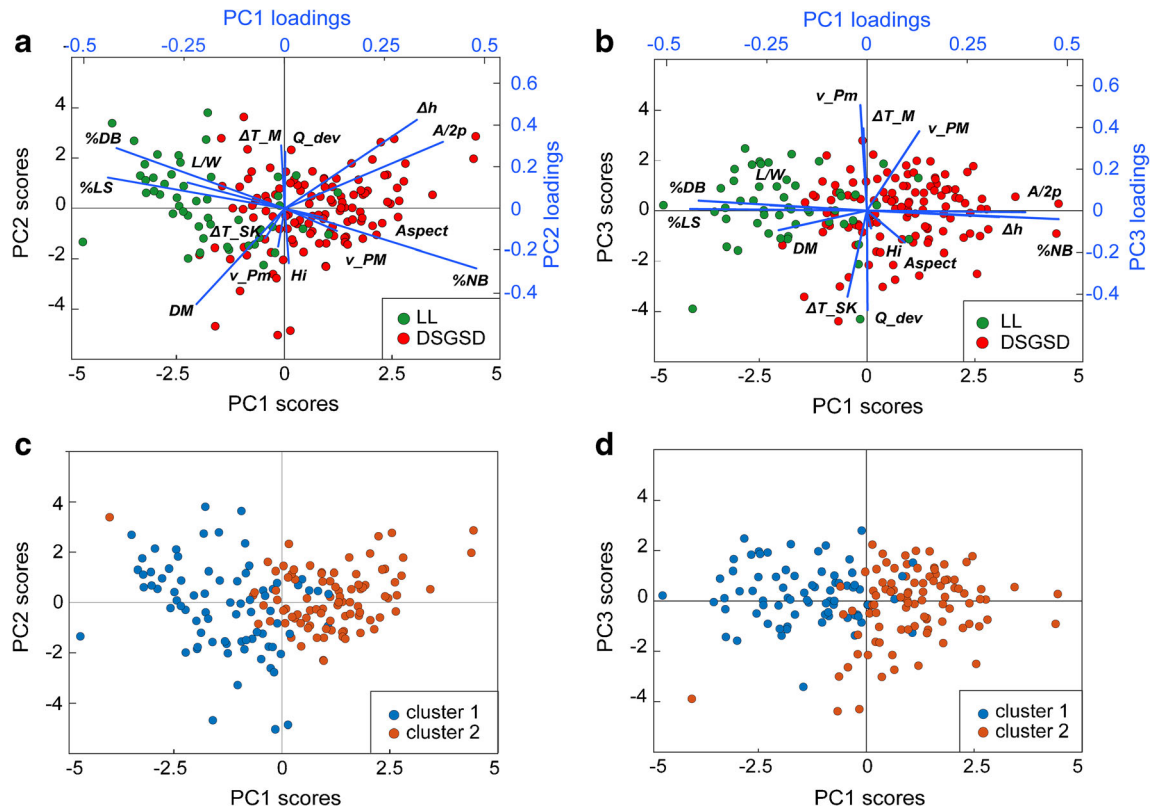


Fig. 6 MV1:PCA and cluster analysis on the SAR covered bulk dataset of rock-slope deformations (DSGSD + large landslides, 166 cases) (a) PC1-PC2 biplot with the result of the PCA and the distribution of DSGSDs (red dots) and Large Landslides (green dots). Blue lines are the eigenvectors corresponding to the input variables. (b) PC1-PC3 biplot resulting from the PCA (c) PC1-PC2 classification plot resulting from a K-medoids analysis run on the PCs scores. The two clusters almost correspond to DSGSD and LL distribution, confirming the distinction between the two groups. (d) PC1-PC3 classification graph resulting from the K-medoids cluster analysis on the PCs scores. The distinction between DSGSDs and LL is evident in both the plots

The resulting two clusters displayed in PC1/PC2 (Fig. 6c) and PC1/PC3 (Fig. 6d) plots are in very good agreement with inventory-based classification into large landslides and DSGSDs.

MV2: all DSGSD and large landslides, morphometric and morpho-structural variables

The second bulk-dataset PCA, considering only morphometric and morpho-structural variables, allows characterizing all the 208 landslides with respect to the first 3 PCs, which account for the 67% of the multivariate space variance.

Most morphometric variables (CB, NB, LS, Δh , A/2p, DM) are related to PC1 and PC2 (Fig. 7a), while elongation ratio (L/W) and hypsometry (Hi) mainly influence PC3 (Fig. 7b).

Cluster analysis with PC1, PC2 and PC3 as input variables and a 3-cluster partition of the dataset define three main groups, namely: *gm1*, *gm2* and *gm3*. The first cluster (*gm1*, Fig. 7c,d) includes landslides with high density of deformed nested bodies (DB) and well-developed scarp areas (LS), testifying significant accumulated deformation. The cluster *gm2* (Fig. 7c,d) includes both large landslides and DSGSD with high values of elongation ratio L/W and affecting a relatively immature topography (high Hi). The third cluster (*gm3*) mainly includes DSGSDs affecting entire high-relief

slopes and characterized by high density of immature nested bodies (NB). These clusters are mainly classified according to PC1, as their boundaries are almost parallel to PC3 axis in the PC1-PC3 plot (Fig. 7c,d).

MV3: DSGSD covered by InSAR data, all variables

This PCA allows establishing links between morphometric, morpho-structural and activity characteristics in DSGSD areas covered by Sentinel InSAR data. These are characterized by high areal PS and pseudo-PS (mean density 43 PS/km²), with a maximum of 259/km² in a single DSGSD. We analyse PCA results considering the first three PCs, which account for 50.2% of variance.

Again, PC1 and PC2 are related to morpho-structural and morphometric information (Fig. 8a). When cases are classified according to their kinematics, the PC1/PC2 plot (Fig. 8b) shows a clear trend from the left to the right hand, corresponding to a shift from translational to roto-translational and rotational mechanisms, in agreement with the orientation of Δ skewness (Δ_{SK}) and Δ median (Δ_{M}) eigenvectors. A trend in the PC space can be also found by classifying cases by their modal velocity, respectful of segmentation effects and ranging between 2 and 21 mm/yr towards

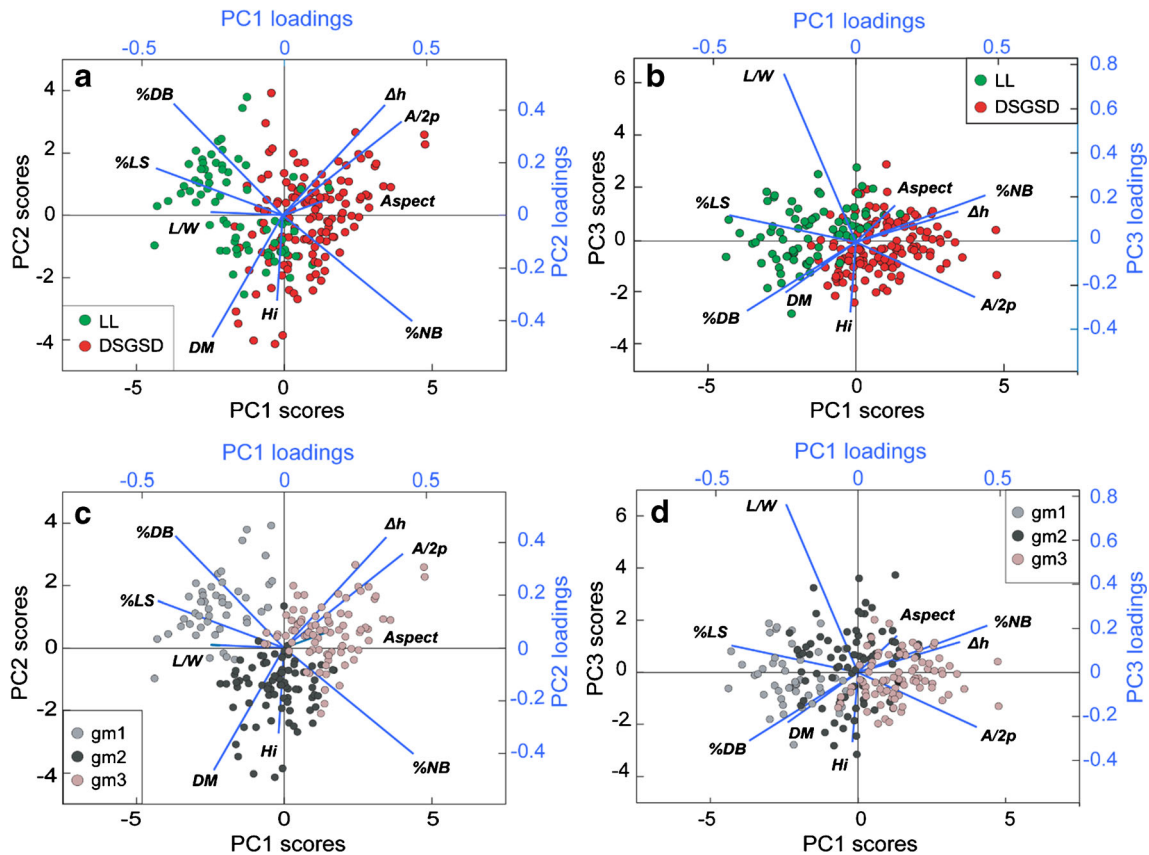


Fig. 7 MV2:PCA and cluster analysis on the entire bulk dataset (208 elements) considering 5 morphometric and 4 morpho-structural variables. (a) and (b) are the PC1-PC2 and PC1-PC3 biplots deriving from a PCA on the whole dataset considering only morphometric and morpho-structural variables. A distinction between inventory based DSGSDs and LL is still evident. (c) and (d) are the result of a 3 clusters K-medoids analysis on the PCs scores. *gm1*, *gm2* and *gm3* are the resulting groups and all the 208 mapped slow rock-slope deformations can be classified in one of them

the upper left of the PC1/PC2 plot (Fig. 8c). In general, translational DSGSDs move faster than rotational and roto-translational ones.

These relationships are outlined in a five-class K-medoids classification, based on PCs as input variables in which the resulting groups (*gc1* to *gc5*) have consistent morphometric and morpho-structural characteristics and represent different styles of activity, illustrated by the arrows in Fig. 8d, which are oriented as the corresponding variables eigenvectors. Cluster *gc1* includes the fastest DSGSDs, characterized by translational kinematics and hosting deformed nested bodies undergoing differential evolution. Clusters *gc2* and *gc3* include slower DSGSDs, significantly segmented but with different kinematics (*gc2* mainly translational, *gc3* mainly rotational) and internal deformation (*gc2* characterized by distributed damage, *gc3* hosting deformed nested sectors). Finally, clusters *gc4* and *gc5* include slow-moving DSGSDs with mainly roto-translational to rotational kinematics, limited internal damage and immature nested bodies.

MV4: large landslides covered by InSAR data, all variables

The same procedure used in MV3 allows classifying large landslides. These usually affect densely vegetated middle-lower slope sectors; therefore, the areal density of PS and pseudo-PS in these

areas is quite low (35PS/km² on average), with a maximum of 163 PS/km² in a single landslide. PCA interpretation is based on the first three PCs accounting for the 47.2% of variance (Fig. 9a).

The PC1-PC2 plot shows a weak trend with respect to landslide kinematics, with a dominantly translational behaviour on the left and a mainly rotational/roto-translational one to the right (Fig. 9b). Similar distribution is found for other variables such as the densities of immature nested bodies (NB) and deformed nested bodies (DB), mainly related to PC1. Activity-related variables, like velocity quartile deviation (*Q_dev*) and modal LOS velocity (*v_PM*), are oriented almost perpendicular to PC1 (Fig. 9a) without any clear velocity trend (Fig. 9c).

Because of the small number of input variables, K-medoids cluster classification only considers two groups, to avoid over splitting the sparse dataset. The groups (Fig. 9d) are mainly discriminated by PC1 values and defined by the density of immature nested bodies (NB) and deformed nested bodies (DB).

MV5: DSGSD and large landslides lacking InSAR data, proximity analysis

Since 42 out of 208 rock-slope deformation lack significant InSAR data coverage, they are not classified in the MV3 and MV4 analyses but only in MV2, based on morphometric and morpho-structural variables and lacking InSAR activity measurements. A two-step

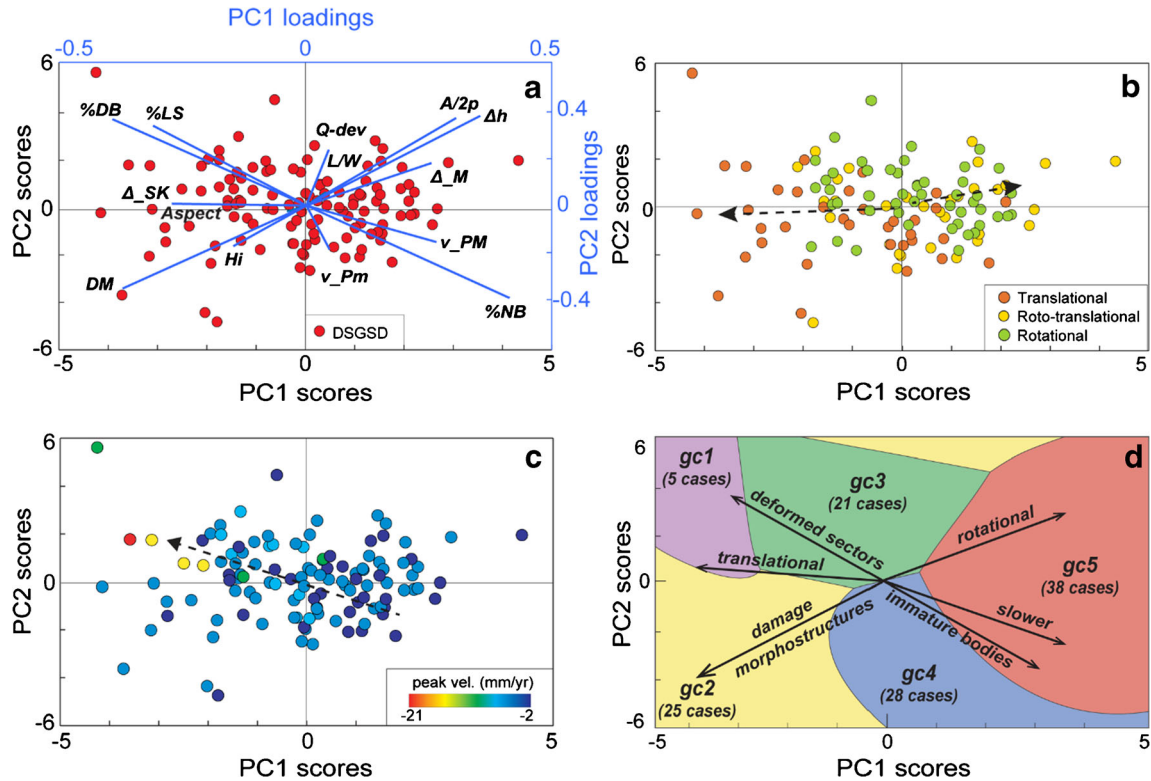


Fig. 8 MV3: combined PCA and cluster analysis for DSGSD covered by InSAR data (117 cases), (a) PC1-PC2 biplot resulting from a PCA on morphometric, morphostructural and InSAR-derived variables. (b) kinematics distribution in the PC1-PC2 plot showing a trend from rotational to translational style from the right to the left side. (c) velocity distribution in the PC1-PC2 plot outlining an increasing velocity trend from the bottom right corner to the upper left one. The coloured fields correspond to the groups identified by a 5 cluster K-medoids analysis on the PCs scores. Boundaries between groups are set according to quadratic discriminant analysis surfaces. Arrows correspond to the direction of representative eigenvectors

proximity analysis is then performed to obtain a complete classification of all the mapped landslides. First, all the mapped landslides were classified in the three main groups extracted from MV2 (gm_1 , gm_2 , gm_3 ; Fig. 10) and displayed in a PC1-PC2 plot. Then, all landslides with InSAR data belonging to the different gm groups were further reclassified in terms of the style of activity classes resulting from MV3 and MV4 (Figs. 8 and 9). Eventually, the 42 SAR-blind cases were reclassified through a proximity analysis considering the surrounding points (minimum Euclidean distance) and their class signature (Fig. 10).

Discussion

Redefining the activity of slow rock-slope deformations

Despite the apparent simplicity of the concept (Cruden and Varnes 1996), a comprehensive definition of “activity” for complex, slow rock-slope deformations remains elusive. A definition only based on a representative displacement rate can be insufficient to capture the behaviour of slope instabilities evolving over thousands of years (Agliardi et al. 2013, 2019a, b; Pánek and Klimeš 2016), for which present-day displacement rates are just a snapshot of longer or variable trends (Riva et al. 2018). Moreover, different phenomena moving at similar rates can have different impacts on elements at risk, depending on their size, mechanisms, maturity and predisposition to collapse (Agliardi et al. 2020; Peduto et al. 2017; Nappo et al. 2019).

We propose that a complete definition of the style of activity of large slow rock-slope deformations must include different aspects, namely: displacement rate, segmentation/heterogeneity, kinematics, internal damage and accumulated strain.

Since slow rock-slope deformations are widespread in mountain ranges and especially in alpine areas, we need to quantify such style of activity on the regional scale, to perform a cost-effective screening of the different landslides’ evolutionary characters and orient further hazard assessment analyses or local-scale engineering geological studies. To do this, we develop a novel approach that combines information derived from persistent scatterer interferometry and from ad hoc systematic geomorphological mapping, to obtain an objective description of the mapped phenomena.

Our analysis benefits from both deterministic and statistical components. The deterministic component consists of original routines in Matlab™ (i.e. peak analysis for the segmentation analysis and 2DInSAR decomposition and machine learning approach for a kinematic assessment) and GIS (semi-detailed mapping and extraction of morphometric and morphological variables) that allow quantifying the internal segmentation, heterogeneity, kinematics and representative displacement rates of each mapped landslide, through a refined post-processing of persistent-scatterer datasets validated using geomorphological mapping. These routines can be used as stand-alone tools and provide variables that, together with morphometric and morphostructural variables, feed a multivariate statistical analysis aimed at

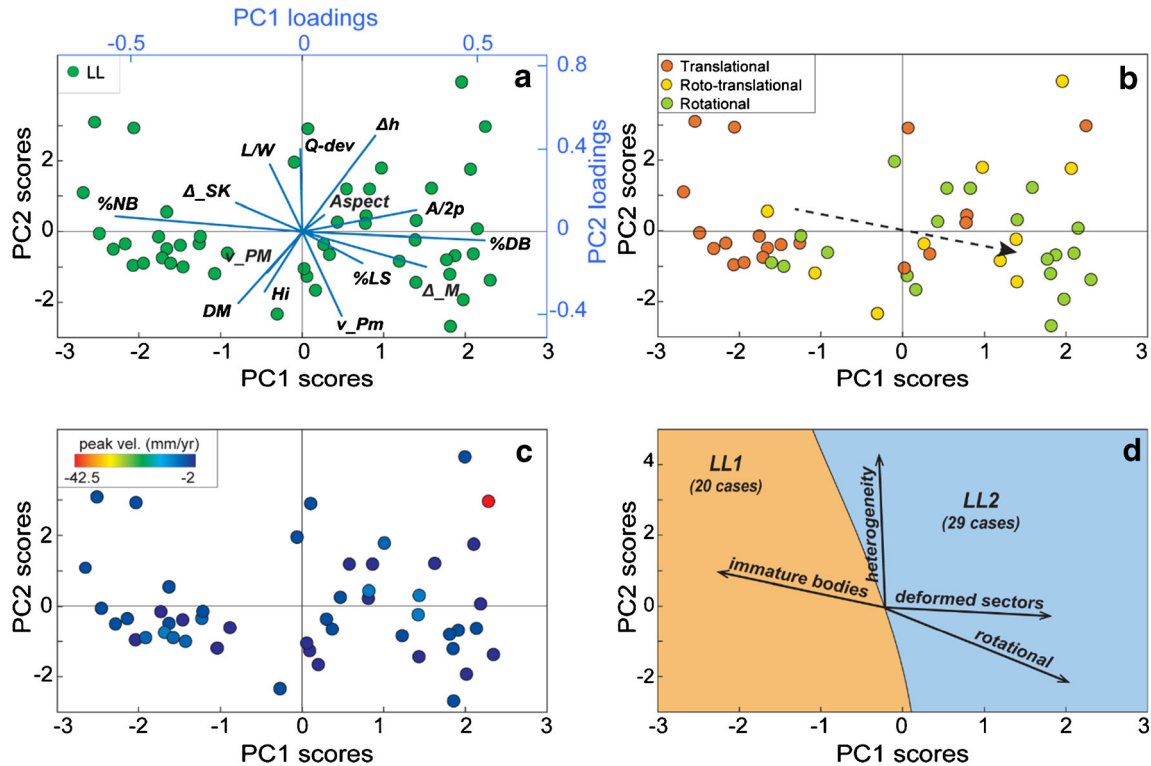


Fig. 9 MV4: combined PCA and cluster analysis for Large Landslides (LL) covered by InSAR data (49 cases). (a) PC1-PC2 biplot resulting from a PCA on morphometric, morpho-structural and InSAR-derived variables. (b) kinematics distribution in the PC1-PC2 plot showing a trend from rotational to translational style from the left to the right side. (c) Velocity distribution in the PC1-PC2 plot outlining an almost homogeneous velocity range with only an extreme values reaching -40mm/yr. (d) classification graph in which the coloured fields correspond to the groups identified by a 2 cluster K-medoids analysis on the PCs scores. Boundaries between groups are set according to quadratic discriminant analysis surfaces. Arrows correspond to the direction of representative eigenvectors

classifying the mapped landslides in groups with consistently different styles of activity.

Objective characterization of segmentation and kinematics from PSI data

Despite the common application of persistent scatterer data to the assessment of landslide activity (Ambrosi and Crosta 2006; Colesanti et al. 2006; Frattini et al. 2018), a full exploitation of their potential for slow rock-slope deformations remains challenging, because of the low signal-to-noise ratio, heterogeneity and complex displacement patterns that can be hardly caught by sparse or unfavourably oriented PS data (Fig. 2). Some authors (Meisina et al. 2008; Notti et al. 2014; Frattini et al. 2018; Aslan et al. 2020) deal with these problems under the assumption of simplified mechanisms (i.e. dominant slope-parallel displacements) not respectful of the complexity of slow rock-slope deformations. The common “unbiased” representation of landslide activity by means of LOS velocity projection along slope (V_{slope} ; Notti et al. 2012, 2014; Aslan et al. 2020) facilitates the interpretation of V_{LOS} data, but hampers any interpretation of global landslide kinematics (Meisina et al. 2008; Frattini et al. 2018).

Also, when exploiting multi-geometry 2DInSAR techniques (Manzo et al. 2006; Dalla Via et al. 2012; Eriksen et al. 2017; Crippa et al. 2020) that allow deriving the vertical and horizontal components of the 2D velocity vector lying in the E-W vertical plane, the assessment of landslide kinematics is not

straightforward. In fact, (a) objective criteria are needed to integrate point-like scatterer information within a global interpretation; (b) internal segmentation affects landslide displacement patterns. We tackle these problems sequentially in a semi-automated workflow.

First, we objectively assess landslide segmentation, i.e. partitioning of slope deformation into discrete nested sectors with differential evolution (Fig. 3). Since a mean landslide LOS velocity (Fig. 5b), computed on all the active PS, potentially mixes signals from discrete landslide sector as well as scattered noise, we use a peak analysis of the velocity frequency distribution to identify the occurrence of segmentation within the main landslide mass (Fig. 5a). The highest peak (Fig. 3), corresponding to the modal LOS velocity, is a representative descriptor of the displacement rate of the main landslide mass (Fig. 5c). Lower (i.e. less frequent) peaks (Fig. 3) outline the signals of discrete nested sectors emerging from the background displacement signals and from scattered noise.

Our method’s ability to outline segmentation is influenced by the abundance and homogeneity of PS and DS in nested sectors (Online Resource Fig. S1, Fig. S4) and by the frequency threshold values used in the peak analysis. Thus, the number of sectors in Fig. 5a must be regarded as a lower-bound estimate. At the same time, our analysis is unable to detect fast-moving landslides within slow rock-slope deformation, due to the temporal baselines of PS-InSARTM and SqueeSARTM analyses processed on the regional scale.

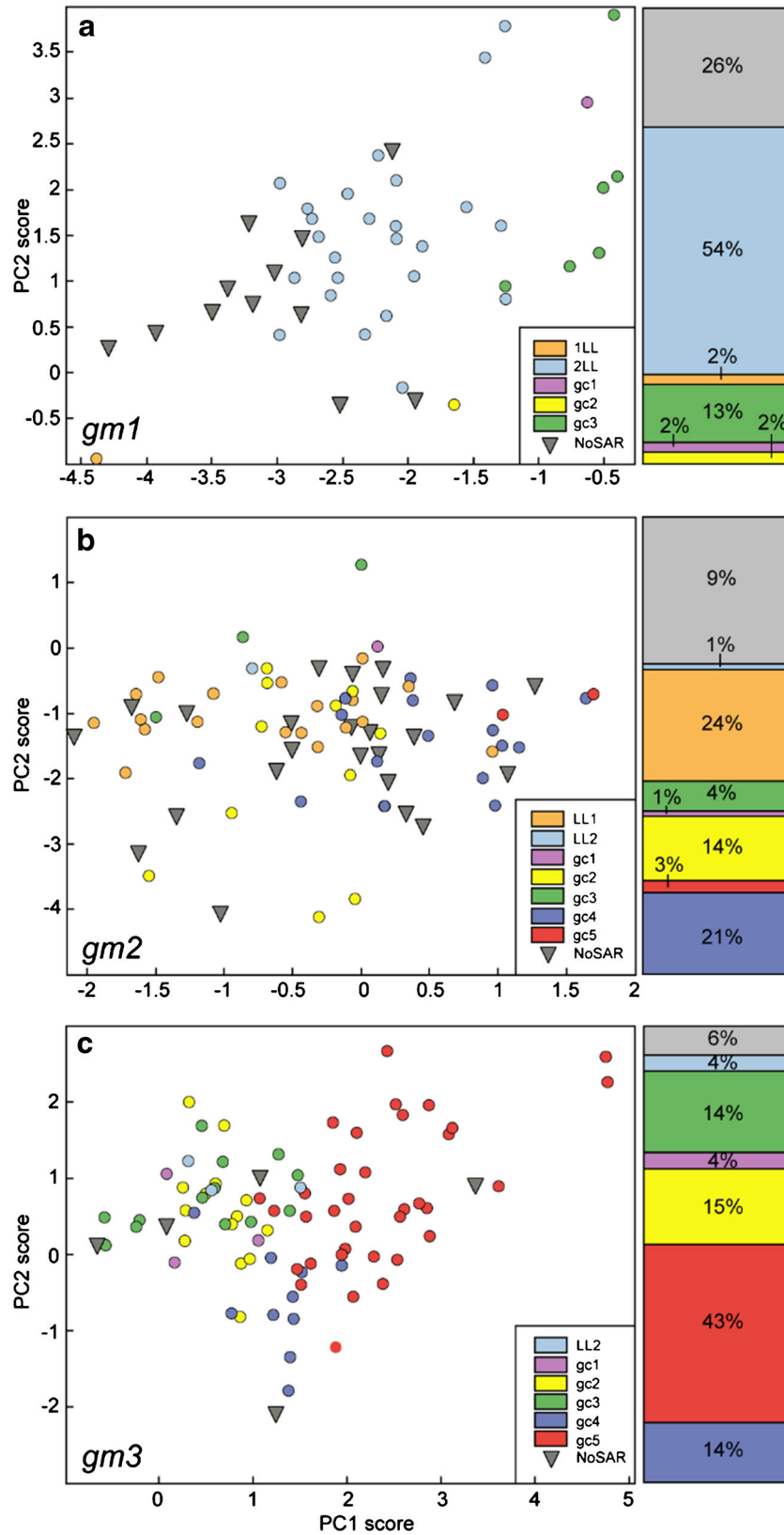


Fig. 10 MV5: proximity analysis on DSGSDs and large landslides not covered by InSAR data (42 cases) according to similarity criteria (Euclidean distance) with the other style of activity classes. (a) shows the distribution of SAR blind elements in gm1, (b) the distribution in gm2 and (c) the distribution in gm3. The stacked column indicates the percentage of each group inside gm1, gm2 and gm3

To achieve an objective evaluation of landslide kinematics, we combine measures from ascending and descending datasets to reconstruct the 2D total displacement vector in the vertical E-W plane. The difference Δ between the inclination (τ) of this displacement vector and the local slope angle allows identifying cells with movements dipping in the slope, parallel to the slope, or daylighting. The statistical distribution of Δ (Fig. 4) over each landslide area provides a signature of its global kinematics. This evaluation of landslide kinematics is biased at slopes where real displacements diverge from the LOS directions, due to slope aspect (i.e. north- or south-facing slopes; Fig. 2b) or to oblique slope movements, and cannot be completely read by the radar sensor (Fig. 2c) due to the intrinsic geometrical limitations of spaceborne SAR platforms. A precise quantification of such bias requires information from additional LOS direction (e.g. other satellite tracks; UAV-SAR ad hoc acquisitions, Hu et al., 2020; GPS or pixel offset tracks), usually unavailable in regional-scale studies, or the a priori knowledge of landslide kinematics, which is our unknown. As we depart from the LOS plane, we can generally expect to underestimate the 2D displacement vector inclination, resulting in a less effective detection of rotational movements. Nonetheless, our proposed approach is suitable for a regional-scale objective screening of landslide kinematics, providing guidance to further local-scale studies.

Our analysis approach can be applied to other large landslide datasets, provided that InSAR data with suitable quality is available and, at the same time, provides information useful for the site-specific characterization of individual landslides.

Style of activity classification of slow rock-slope deformations

A practical evaluation of the style of activity of slow rock-slope deformation for land planning, hazard assessment and engineering purposes must account for a suite of kinematic, morphometric and morpho-structural descriptors. Our multivariate statistical analysis allows classifying the studied dataset into 7 groups with fairly homogeneous styles of activity, even including cases for which InSAR data are unavailable to describe the present-day patterns of movement.

First, our results (MV1) outline clear differences between DSGSD and large landslide phenomena according to the considered variables. This is not obvious, because the distinction between these two classes of slope instability is debated and usually only relies on morphometric and morpho-structural criteria, including the affected relief and slope sectors, morpho-structural expression and total accumulated strain (Crosta et al. 2013). On the other hand, the very similar magnitude-frequency scaling of hundreds of DSGSD and large landslides suggests that the two classes of phenomena belong to a continuous spectrum of slow rock-slope deformations, where the diagnostic features used for their distinction are constrained by size (Agliardi et al. 2012). Interestingly, multivariate statistical analysis provides a sharp distinction in two groups, well-fitting the geomorphological pre-classification into DSGSDs and large landslides (Fig. 6). More elongated shapes and high density of deformed nested bodies, testifying higher accumulated internal deformation, characterize large landslides with respect to DSGSDs (Fig. 7). This suggests that DSGSDs and large landslides undergo different mechanisms and/or evolutionary stages and should be treated separately.

Multivariate statistical analyses, performed on DSGSD and large landslides separately (MV3 and MV4) and expanded through a similarity analysis to include SAR-blind landslides (MV5), led to the classification of the landslide inventory into seven style-of-activity classes, five for DSGSDs and two for large landslides. The distributions of the different variables in each group (boxplots in Online Resource Fig. S5) demonstrate the impossibility to use single variables as reliable indicators of the style of activity of slow rock-slope deformations.

Furthermore, the concept of “inactive” landslides implies a capability to correctly measure displacements at all sites, not guaranteed by InSAR techniques due to (a) the inability of radar sensors to illuminate unfavourably oriented slopes and (b) the lack of coherence of interferograms in densely vegetated or debris covered slopes. Since we cannot be sure that SAR-blind landslides are not moving, to avoid underestimation of the related risks, we dropped the concept of “inactive landslides” and classified all the cases in the seven style-of-activity classes.

Our classification provides an accurate mapping (Fig. 11) of slow rock-slope deformations with consistent style of activity. This is useful to identify critical phenomena to prioritize site-specific analyses and to analyse the damage potential of slow rock-slope deformations on specific classes of elements at risk, depending on the most important interaction factors (e.g. rate, volume, heterogeneity).

The class *gc1* includes the fastest DSGSDs (5, all covered by InSAR data; Fig. 11), typically affecting high relief slopes (>1200 m) and characterized by dominant translational kinematics (Fig. 8 and Online Resource Fig. S5). These DSGSDs evolve at modal rates up to 15–20 mm/yr and host deformed nested bodies that undergo faster differential evolution at displacement rates exceeding 25 mm/yr (Online Resource Fig. S5). This class includes the most active DSGSDs in Lombardia (i.e. Corna Rossa, Agliardi et al. 2018, 2019a; Saline, Agliardi et al. 2001; Mt. Mater, Crippa et al. 2020; 11, 10 and 3, respectively, in Fig. 11), that pose major risk to infrastructures (roadways, hydroelectric facilities and lifelines). These are the most important candidates for site-specific studies to quantify their potential for slow-to-fast evolution and catastrophic failure (Crosta et al. 2017; Agliardi et al. 2020).

The other classes include far slower landslides (i.e. modal and mean LOS velocities lower than 5–10 mm/yr) that cannot be distinguished in terms of displacement rates (Online Resource Fig. S5), but are characterized by different mechanisms and degrees of segmentation, internal damage and accumulated strain (Online Resource Figs. S5 and 11). Clusters *gc2* (32 DSGSD, including 7 SAR-blind cases) and *gc3* (21 DSGSD; Fig. 11) include phenomena affecting middle-high relief slopes and characterized by significant segmentation, but with different kinematics and internal deformation style. *gc2* are dominantly translational and characterized by significant distributed damage (e.g. Bosco del Conte DSGSD; (Agliardi et al. 2009); Fuipiano DSGSD; (Forcella, 1984); 8 and 14, respectively, in Fig. 11), while *gc3* are dominantly rotational and segmented into deformed nested sectors (e.g. Masuccio DSGSD, (De Finis et al., 2015); 6 in Fig. 11). Although these DSGSDs are slow, their strong heterogeneity must be considered in practical engineering geological problems including (a) the definition of potential collapse scenarios, i.e. actually evolving nested volumes constrained by

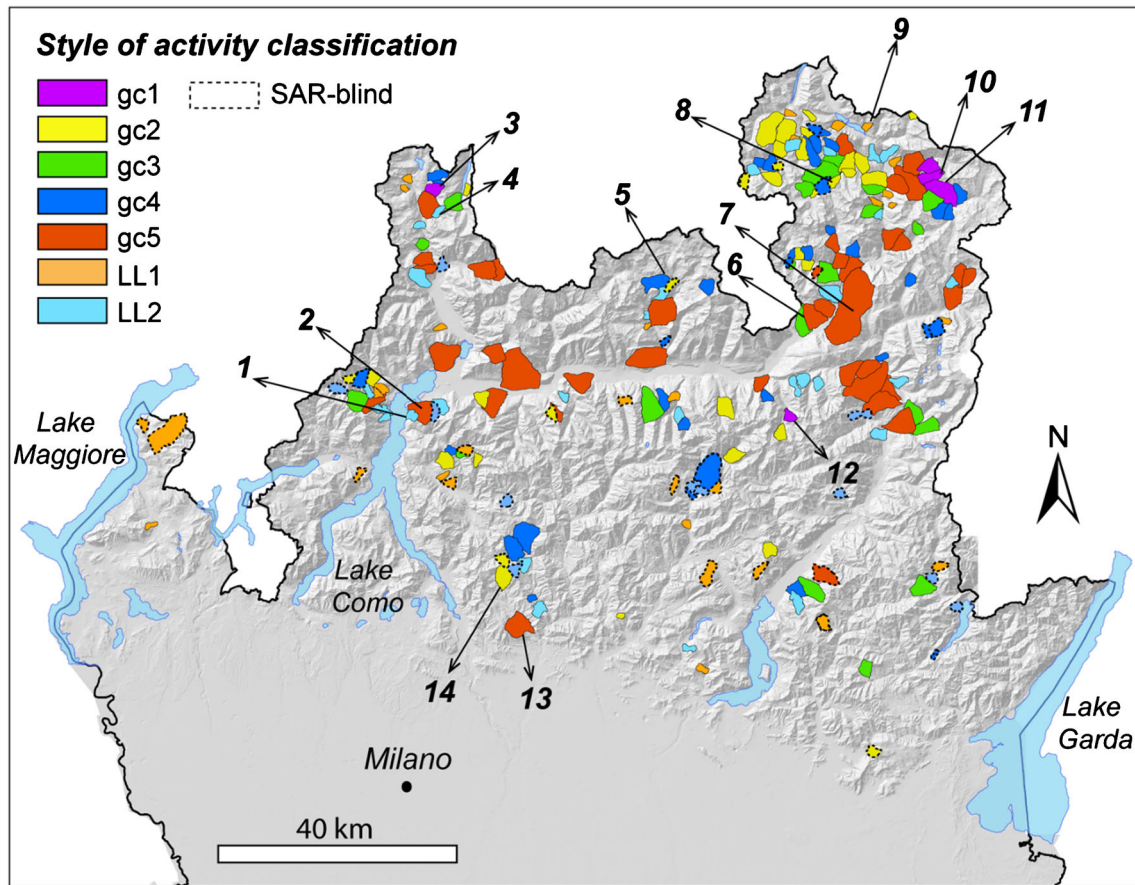


Fig. 11 Style of activity classification map of slow rock-slope deformations in Lombardia. Mapped cases are classified in the seven group arising from the multivariate statistical analysis. Key to the case studies cited in the text: 1: Mt. Letè (Cancelli 2017); 2: Mt Legnone DSGSD (Ambrosi and Crosta, 2006); 3: Mt. Mater DSGSD (Crippa et al., 2020); 4: Piz Groppera large landslide; 5: Lake Palù DSGSD (Frattini et al., 2013); 6: Mt. Masuccio DSGSD (De Finis et al. 2015) 7: Padrio-Varadega DSGSD (Forcella 1984; Ambrosi and Crosta 2006; Frattini et al. 2013); 8: Bosco del Conte DSGSD (Agliardi et al. 2009); 9: Mt Solena large landslide; 10: Saline DSGSD (Agliardi et al., 2001; Frattini et al., 2018; Agliardi et al., 2018); 11: Corna Rossa DSGSD (Agliardi et al., 2018); 12: Belviso DSGSD; 13: Albenza (Forcella 1987); 14: Fuipiano DSGSD (Forcella and Rossi 1987)

segmentation; (b) the quantification of rock mass properties for stability modelling, strongly depending on internal damage; and (c) the prediction of damage to infrastructures that is significantly complicated by differential displacements in heterogeneous landslide masses. Finally, classes *gc4* (38 DSGSD, including 10 SAR-blind cases) and *gc5* (40 DSGSD, including 2 SAR-blind cases) include slow-moving DSGSDs characterized by either dominant roto-translational (*gc4*; e.g. Lake Palù DSGSD (Frattini et al., 2013); 5 in Fig. 11) or rotational kinematics (*gc5*; e.g. Albenza DSGSD; (Forcella, 1987) 13 in Fig. 11). Both classes include phenomena with limited internal damage and segmentation into poorly deformed nested bodies (Online Resource Fig. S5).

Style of activity classes defined for large landslides, i.e. *LL1* (32 large landslides, including 12 SAR-blind cases) and *LL2* (40 large landslides, including 11 SAR-blind cases), differs according to morpho-structural characteristics that witness different geomorphological maturities and accumulated deformations (Online Resource Fig. S5). In particular, class *LL1* (e.g. Mt. Solena; 9 in Fig. 11) includes translational landslides affecting slopes with relatively low relief (Online Resource Fig.

S5), characterized by limited scarp areas and segmented into immature nested masses, suggesting a limited accumulated strain. Instead, class *LL2* (e.g. Pizzo Groppera; 4 in Fig. 11) mainly includes roto-translational and rotational landslides, affecting high-relief slopes and characterized by large accumulated deformations.

Conclusions

Slow rock-slope deformations are widespread in alpine valleys. Despite their limited displacement rates (mm to few cm per year), these phenomena are long-lived and deform slowly, possibly until massive sector collapse, posing major risks to infrastructures and human lives. Our regional-scale analysis allows performing a complete screening of ongoing slow rock-slope deformations, with the following results:

- New semi-automated, objective methods and tools to characterize the internal segmentation and kinematics of slow rock-slope deformations. These methods, readily applicable to other datasets, highlight phenomena subjected to a certain degree of segmentation, with the presence of internal nested bodies that

can potentially evolve into faster landslides, and their global kinematics.

- A statistically based evidence that DSGSD and large landslides have different mechanisms and/or evolutionary stages, with different associated morphological features that testify higher accumulated internal deformation for large landslides with respect to DSGSD.
- A statistically based classification of slow rock-slope deformations based on their style of activity, including the contributions of displacement rate, segmentation, kinematics and internal damage. This classification supports regional-scale land planning and the prioritization of detailed site-specific mapping, monitoring and modelling studies, required to understand and deal with issues posed by slow rock-slope deformations.

Acknowledgements

The authors are indebted with Matteo Andreozzi, Simona Imperiali, Roberta Schibuola and Michela Cincera for contributing to geomorphological mapping. We thank Dr. Andrea Manconi for fruitful discussions on the potential and limitations of regional-scale InSAR applications and Marco Previtali for its tips and tricks with Matlab programming. We are also indebted to Massimo Ceriani (Regione Lombardia) for providing some PS datasets.

The research was supported by Fondazione Cariplo grant 2016-0757 “Slow2Fast” to F. Agliardi and by the MIUR–“Dipartimenti di Eccellenza 2018–2022, Department of Earth and Environmental Sciences, University of Milano-Bicocca”.

Author contribution

C. Crippa and F. Agliardi conceived the research and wrote the paper. E. Valbuzzi, F. Agliardi and M. Spreafico edited the geomorphological mapping dataset. C. Crippa performed InSAR data analysis and multivariate statistical analysis. P. Frattini contributed to statistical analysis. P. Frattini and G.B. Crosta revised the paper and contributed to the discussion.

Funding

Open access funding provided by Università degli Studi di Milano - Bicocca within the CRUI-CARE Agreement.

Open Access This article is licensed under a Creative Commons Attribution 4.0 International License, which permits use, sharing, adaptation, distribution and reproduction in any medium or format, as long as you give appropriate credit to the original author(s) and the source, provide a link to the Creative Commons licence, and indicate if changes were made. The images or other third party material in this article are included in the article's Creative Commons licence, unless indicated otherwise in a credit line to the material. If material is not included in the article's Creative Commons licence and your intended use is not permitted by statutory regulation or exceeds the permitted use, you will need to obtain permission directly from the copyright holder. To view a copy of this licence, visit <http://creativecommons.org/licenses/by/4.0/>.

References

- Agliardi F, Crosta G, Zanchi A, Agliardi F, AZ GC (2001) Structural constraints on deep-seated slope deformation kinematics. *Eng Geol* 59:83–102. [https://doi.org/10.1016/S0013-7952\(00\)00066-1](https://doi.org/10.1016/S0013-7952(00)00066-1)
- Agliardi F, Zanchi A, Crosta GB (2009) Tectonic vs. gravitational morphostructures in the central Eastern Alps (Italy): constraints on the recent evolution of the mountain range. *Tectonophysics* 474:250–270. <https://doi.org/10.1016/j.tecto.2009.02.019>
- Agliardi F, Crosta GB, Frattini P (2012) Slow rock-slope deformation. In: *Landslides: Types, mechanisms and modeling*. Cambridge University Press, Cambridge, p 207
- Agliardi F, Crosta GB, Frattini P, Malusà MG (2013) Giant non-catastrophic landslides and the long-term exhumation of the European Alps. *Earth Planet Sci Lett* 365:263–274. <https://doi.org/10.1016/j.epsl.2013.01.030>
- Agliardi F, Spreafico MC, Zanchetta S et al (2018) Gravitational transfer zones influence DSGSD mechanisms and activity. *EGUGA* 13819
- Agliardi F, Crippa C, Spreafico MC, Manconi A, Bourlès D, Braucher R, Cola G, Zanchetta S (2019a) Strain partitioning and heterogeneous evolution in a giant slope deformation revealed by InSAR, dating and modelling. In: *Geophysical Research Abstracts*
- Agliardi F, Riva F, Barbarano M, Zanchetta S, Scotti R, Zanchi A (2019b) Effects of tectonic structures and long-term seismicity on paraglacial giant slope deformations: Piz Dora (Switzerland). *Eng Geol* 263:105353. <https://doi.org/10.1016/j.enggeo.2019.105353>
- Agliardi F, Scuderi MM, Fusi N, Collettini C (2020) Slow-to-fast transition of giant creeping rockslides modulated by undrained loading in basal shear zones. *Nat Commun* 11:1–11. <https://doi.org/10.1038/s41467-020-15093-3>
- Allievi J, Ambrosi C, Ceriani M, Colesanti C, Crosta GB, Ferretti A, Fossati D (2003) Monitoring slow mass movements with the permanent scatterers technique. In: *IGARSS 2003. 2003 IEEE International Geoscience and Remote Sensing Symposium. Proceedings (IEEE Cat. No. 03CH37477)*. IEEE, pp 215–217
- Ambrosi C, Crosta GB (2006) Large sackung along major tectonic features in the Central Italian Alps. *Eng Geol* 83:183–200. <https://doi.org/10.1016/j.enggeo.2005.06.031>
- Arora P, Varshney S (2016) Analysis of K-means and K-medoids algorithm for big data. *Proc Comput Sci* 78:507–512. <https://doi.org/10.1016/j.procs.2016.02.095>
- Aslan G, Fournelis M, Raucoules D, De Michele M, Bernardie S, Cakir Z (2020) Landslide mapping and monitoring using persistent scatterer interferometry (PSI) technique in the French alps. *Remote Sens* 12. <https://doi.org/10.3390/RS12081305>
- Audemard FA, Beck C, Carrillo E (2010) Deep-seated gravitational slope deformations along the active Boconó Fault in the central portion of the Mérida Andes, western Venezuela. *Geomorphology*. 124:164–177. <https://doi.org/10.1016/j.geomorph.2010.04.020>
- Ballabio D (2015) A MATLAB toolbox for principal component analysis and unsupervised exploration of data structure. *Chemom Intell Lab Syst* 149:1–9. <https://doi.org/10.1016/j.chemolab.2015.10.003>
- Ballabio D, Consonni V (2013) Classification tools in chemistry. Part 1: Linear models. *PLS-DA. Anal Methods* 5:3790–3798. <https://doi.org/10.1039/c3ay40582f>
- Bianchini S, Pratesi F, Nolesini T, Casagli N (2015) Building deformation assessment by means of persistent scatterer interferometry analysis on a landslide-affected area: the Volterra (Italy) case study. *Remote Sens* 7(4):4678–4701
- Bini A, Buoncristiani J-F, Couterrand S, Ellwanger D., Felber M., Florineth D., Graf H.R., Keller O., Kelly M., Schlüchter C. and Schoeneich P. (2009) Die Schweiz während des letzteiszeitlichen Maximums (LGM). Bundesamt für Landestopographie, swisstopo
- Bovis MJ (1990) Rock-slope deformation at Affliction Creek, southern Coast Mountains, British Columbia. *Can J Earth Sci* 27:243–254. <https://doi.org/10.1139/e90-024>
- Bovis MJ (2013) Sackung. In: *Geological Society of America Bulletin*. pp 881–882
- Brückl E, Brunner FK, Kraus K (2006) Kinematics of a deep-seated landslide derived from photogrammetric, GPS and geophysical data. *Eng Geol* 88:149–159. <https://doi.org/10.1016/j.enggeo.2006.09.004>
- Brückl E, Brunner FK, Lang E, Mertl S, Müller M, Stary U (2013) The Gradenbach Observatory—monitoring deep-seated gravitational slope deformation by geodetic, hydrological, and seismological methods. *Landslides* 10:815–829. <https://doi.org/10.1007/s10346-013-0417-1>
- Ceriani M, Fossati D (2005) *Inventario dei Fenomeni Franosi in Lombardia Regione Lombardia*. DG Protezione civile, Programma delle Ricerche Strategiche
- Chigira M (1992) Long-term gravitational deformation of rocks by mass rock creep. *Eng Geol* 32:157–184. [https://doi.org/10.1016/0013-7952\(92\)90043-X](https://doi.org/10.1016/0013-7952(92)90043-X)
- Ciampalini A, Solari L, Giannacchini R, Galanti Y, Moretti S (2019) Evaluation of subsidence induced by long-lasting buildings load using InSAR technique and geotechnical data: the case study of a Freight Terminal (Tuscany, Italy). *Int J Appl Earth Obs Geoinf* 82:101925

- Cohen-Waerber J, Bürgmann R, Chaussard E, Giannico C, Ferretti A (2018) Spatiotemporal patterns of precipitation-modulated landslide deformation from independent component analysis of InSAR time series. *Geophys Res Lett* 45:1878–1887
- Colesanti C, Ferretti A, Prati C, Rocca F (2003) Monitoring landslides and tectonic motions with the permanent scatterers technique. *Eng Geol* 68:3–14. [https://doi.org/10.1016/S0013-7952\(02\)00195-3](https://doi.org/10.1016/S0013-7952(02)00195-3)
- Colesanti C, Crosta GB, Ferretti A, Ambrosi C (2006) Monitoring and assessing the state of activity of slope instabilities by the permanent scatterers technique. In: *Landslides from Massive Rock Slope Failure*. Springer, pp 175–194
- Colesanti C, Wasowski J (2006) Investigating landslides with space-borne synthetic aperture radar (SAR) interferometry. *Eng Geol* 88:173–199. <https://doi.org/10.1016/j.enggeo.2006.09.013>
- Crippa C, Franzosi F, Zonca M, Manconi A, Crosta GB, Dei Cas L, Agliardi F (2020) Unraveling spatial and temporal heterogeneities of very slow rock-slope deformations with targeted DInSAR analyses. *Remote Sens* 12:1329. <https://doi.org/10.3390/rs12081329>
- Crosta GB (1996) Landslide, spreading, deep seated gravitational deformation: analysis, examples, problems and proposals. *Geogr Fis Din Quat* 19:297–313
- Crosta GB, Zanchi A (2000) Deep seated slope deformations: huge, extraordinary, enigmatic phenomena. In: *Landslides in Research, Theory and Practice: Proceedings of the 8th International Symposium on Landslides held in Cardiff on 26–30 June 2000*. Thomas Telford publishing, pp 1–351
- Crosta GB, Frattini P, Agliardi F (2013) Deep seated gravitational slope deformations in the European Alps. *Tectonophysics* 605:13–33. <https://doi.org/10.1016/j.tecto.2013.04.028>
- Crosta GB, Agliardi F, Rivolta C, Alberti S, Dei Cas L (2017) Long-term evolution and early warning strategies for complex rockslides by real-time monitoring. *Landslides* 14:1615–1632. <https://doi.org/10.1007/s10346-017-0817-8>
- Cruden DM, Varnes DJ (1996) Landslides: investigation and mitigation. Chapter 3- Landslide types and processes. Transportation research board special report, 247
- Dalla Via G, Crossetto M, Crippa B (2012) Resolving vertical and east-west horizontal motion from differential interferometric synthetic aperture radar: The L'Aquila earthquake. *J Geophys Res Solid Earth* 117. <https://doi.org/10.1029/2011JB008689>
- De Finis E, Gattinoni P, Scesi L (2015) The genesis of the anomalous Semio Fan, Valtellina, Northern Italy. *Int J Civ Environ Eng* 9:1309–1315
- Del Soldato M, Solari L, Raspini F, Bianchini S, Ciampalini A, Montalti R, Ferretti A, Pellegrineschi V, Casagli N (2019) Monitoring ground instabilities using SAR satellite data: a practical approach. *ISPRS Int J Geo Inf* 8. <https://doi.org/10.3390/ijgi8070307>
- Del Ventisette C, Raspini F, Ciampalini A, Di Traglia F, Moscatelli M, Pagliaroli A, Moretti S (2015) Use of PSInSAR data to map highly compressible soil layers. *Geol Acta* 13(4):309–323
- Eriksen HØ, Lauknes TR, Larsen Y, Corner GD, Bergh SG, Dehls J, Kierulf HP (2017) Visualizing and interpreting surface displacement patterns on unstable slopes using multi-geometry satellite SAR interferometry (2D InSAR). *Remote Sens Environ* 191:297–312. <https://doi.org/10.1016/j.rse.2016.12.024>
- Ferretti A, Prati C, Rocca F (2001) Permanent scatterers in SAR interferometry. *IEEE Trans Geosci Remote Sens* 39:8–20. <https://doi.org/10.1109/36.898661>
- Ferretti A, Fumagalli A, Novali F, Prati C, Rocca F, Rucci A (2011) A new algorithm for processing interferometric data-stacks: SqueeSAR. In: *IEEE Transactions on Geoscience and Remote Sensing*
- Fisher RA (1936) The use of multiple measurements in taxonomic problems. *Ann Eugenics* 7:179–188. <https://doi.org/10.1111/j.1469-1809.1936.tb02137.x>
- Florineth D, Froitzheim N (1994) Transition from continental to oceanic basement in the Tasna nappe (Engadine window, Graubünden, Switzerland): evidence for early Cretaceous opening of the Valais Ocean. *Schweiz Mineral Petrogr Mitt* 74:437–448
- Forcella F (1984) The Sacking between Mount Padrio and Mount Varadega, Central Alps, Italy : a remarkable example of slope gravitational tectonics. *Méditerranée* 51:81–92. <https://doi.org/10.3406/medit.1984.2237>
- Forcella F (1987) La deformazione di versante del M. Albenza Boll Soc Geol Ital 106:273–280
- Forcella F, Rossi PM (1987) Le deformazioni di versante presenti nel territorio di Fuipiano Imagna (Prealpi bergamasche). *Boll Soc Geol Ital* 106:281–291
- Frattini P, Crosta GB, Allievi J (2013) Damage to buildings in large slope rock instabilities monitored with the PSInSAR™ technique. *Remote Sens* 5:4753–4773. <https://doi.org/10.3390/rs5104753>
- Frattini P, Crosta GB, Rossini M, Allievi J (2018) Activity and kinematic behaviour of deep-seated landslides from PS-InSAR displacement rate measurements. *Landslides* 15:L1–L18. <https://doi.org/10.1007/s10346-017-0940-6>
- Gabriel AK, Goldstein RM, Zebker HA (1989) Mapping small elevation changes over large areas: differential radar interferometry. *J Geophys Res* 94:9183–9191. <https://doi.org/10.1029/JB094iB07p09183>
- Grämiger LM, Moore JR, Gischig VS, Ivy-Ochs S, Loew S (2017) Beyond debuttering: mechanics of paraglacial rock slope damage during repeat glacial cycles. *J Geophys Res Earth Surf* 122:1004–1036. <https://doi.org/10.1002/2016JF003967>
- Hengl T, Reuter HI (2008) Geomorphometry: concepts, software, applications. *Newnes*
- Hotelling H (1933) Analysis of a complex of statistical variables into principal components. *J Educ Psychol* 24:417–441
- Hu X, Bürgmann R, Fielding EJ, Lee H (2020) Internal kinematics of the Slumgullion landslide (USA) from high-resolution UAVSAR InSAR data. *Remote Sens Environ* 251:112057
- Hungro O, Leroueil S, Picarelli L (2014) The Varnes classification of landslide types, an update. *Landslides* 11(2):167–194
- Ivy-Ochs S, Kerschner H, Reuther A, Preusser F, Heine K, Maisch M, Kubik PW, Schlüchter C (2008) Chronology of the last glacial cycle in the European Alps. *J Quat Sci* 23:559–573. <https://doi.org/10.1002/jqs.1202>
- Jin X, Han J (2010) K-Medoids Clustering BT - Encyclopedia of machine learning. In: Sammut C, Webb GI (eds). Springer US, Boston, pp 564–565
- Kaufman L, and Rousseeuw PJ (1990) Finding groups in data: an introduction to cluster analysis.
- Lebuis J, Robert J-M, Rissmann P (1983) Regional mapping of landslide hazard in Quebec. *Rapp Statens Geotekniska Inst* 17:205–262
- Lin CW, Tseng CM, Tseng YH, Fei LY, Hsieh YC, Tarolli P (2013) Recognition of large scale deep-seated landslides in forest areas of Taiwan using high resolution topography. *J Asian Earth Sci* 62:389–400. <https://doi.org/10.1016/j.jseaes.2012.10.022>
- Mansour Z, Miloud B, Donzé F, Soraya R, Abderahmane H (2015) Morphometric analysis of landslides in the Ouarsenis area (west Algeria): implications for establishing a relationship between tectonic, geomorphologic, and hydraulic indexes. *Arab J Geosci* 8:6465–6482. <https://doi.org/10.1007/s12517-014-1711-5>
- Manzo M, Ricciardi GP, Casu F, Ventura G, Zeni G, Borgström S, Bernardino P, Del Gaudio C, Lanari R (2006) Surface deformation analysis in the Ischia Island (Italy) based on spaceborne radar interferometry. *J Volcanol Geotherm Res* 151:399–416. <https://doi.org/10.1016/j.jvolgeores.2005.09.010>
- Massart DL (1983) The interpretation of analytical chemical data by the use of cluster analysis. No. 04; QD75. 4. S8, M.
- Meisina C, Zucca F, Notti D, Colombo A, Cucchi A, Savio G, Giannico C, Bianchi M (2008) Geological interpretation of PSInSAR Data at regional scale. *Sensors* 8:7469–7492. <https://doi.org/10.3390/s8117469>
- Montrasio A, Bigioggero B, Maino A, Cirese E, Tacchia D (1990) Carta geologica della Lombardia: scala 1: 250.000. Istituto poligrafico e zecca dello stato
- Nappo N, Peduto D, Mavrouli O, van Westen CJ, Gullà G (2019) Slow-moving landslides interacting with the road network: analysis of damage using ancillary data, in situ surveys and multi-source monitoring data. *Eng Geol* 260:105244
- Notti D, Herrera G, Bianchini S, Meisina C, Garcia-Davalillo JC, Zucca F (2014) A methodology for improving landslide PSI data analysis. *Int J Remote Sens* 35:2186–2214. <https://doi.org/10.1080/01431161.2014.889864>
- Notti D, Meisina C, Zucca F, Colombo A (2012, 2011) Models to predict persistent scatterers data distribution and their capacity to register movement along the slope. *Proc FRINGE* 2011:19–23
- Pánek T, Břežný M, Kapustová V, Lenart J, Chalupa V (2019) Large landslides and deep-seated gravitational slope deformations in the Czech Flysch Carpathians: new LiDAR-based inventory. *Geomorphology* 346:106852. <https://doi.org/10.1016/j.geomorph.2019.106852>
- Pánek T, Klimeš J (2016) Temporal behavior of deep-seated gravitational slope deformations: a review. *Earth Sci Rev* 156:14–38. <https://doi.org/10.1016/j.earscirev.2016.02.007>
- Pearson K (1901) LIII. On lines and planes of closest fit to systems of points in space. *London, Edinburgh. Dublin Philos Mag J Sci* 2:559–572
- Pedrazzini A, Humair F, Jaboyedoff M, Tonini M (2016) Characterisation and spatial distribution of gravitational slope deformation in the Upper Rhone catchment (Western Swiss Alps). *Landslides* 13:259–277. <https://doi.org/10.1007/s10346-015-0562-9>
- Peduto D, Ferlisi S, Nicodemo G, Reale D, Pisciotta G, Gullà G (2017) Empirical fragility and vulnerability curves for buildings exposed to slow-moving landslides at medium and large scales. *Landslides* 14:1993–2007
- Radbruch-Hall DH, Varnes DJ, Savage WZ (1976) Gravitational spreading of steep-sided ridges ("sackung") in Western United States. *Bull Int Assoc Eng Geol* 13:23–35. <https://doi.org/10.1007/BF02634754>

- Rainer P, Martin B, Rudolf H, Pavel L (2005) Geomechanics of hazardous landslides. *J Mt Sci* 2:211–217
- Raspini F, Bianchini S, Ciampalini A, Del Soldato M, Solari L, Novali F, Del Conte S, Rucci A, Ferretti A, Casagli N (2018) Continuous, semi-automatic monitoring of ground deformation using Sentinel-1 satellites. *Sci Rep* 8(1):1–11
- Riva F, Agliardi F, Amitrano D, Crosta GB (2018) Damage-based time-dependent modeling of paraglacial to postglacial progressive failure of large rock slopes. *J Geophys Res Earth Surf* 123:124–141. <https://doi.org/10.1002/2017JF004423>
- Rosi A, Agostini A, Tofani V, Casagli N (2014) A procedure to map subsidence at the regional scale using the persistent scatterer interferometry (PSI) technique. *Remote Sens* 6:10510–10522. <https://doi.org/10.3390/rs61110510>
- Rotaru A, Oajdea D, Răileanu P (2007) Analysis of the landslide movements. *Int J Geol* 1:70–79
- Rott H, Scheuchl B, Siegel A, Grasmann B (1999) Monitoring very slow slope movements by means of SAR interferometry: a case study from a mass waste above a reservoir in the Otztal Alps. *Aust Geophys Res Lett* 26:1629–1632. <https://doi.org/10.1029/1999GL900262>
- Saroli M, Stramondo S, Moro M, Doumaz F (2005) Movements detection of deep seated gravitational slope deformations by means of InSAR data and photogeological interpretation: northern Sicily case study. *Terra Nova* 17:35–43
- Schlögel R, Doubre C, Malet JP, Masson F (2015) Landslide deformation monitoring with ALOS/PALSAR imagery: a D-InSAR geomorphological interpretation method. *Geomorphology* 231:314–330. <https://doi.org/10.1016/j.geomorph.2014.11.031>
- Schmid SM, Fügenschuh B, Kissling E, Schuster R (2004) Tectonic map and overall architecture of the Alpine orogen. *Eclogae Geol Helv* 97:93–117. <https://doi.org/10.1007/s00015-004-1113-x>
- Schmid SM (2017) On the Insubric line and the Southern Steep Belt of the Penninic nappes in the Ticino area (including 2 excursion guides). *Swiss Bull Appl Geol* 22(2):69–89
- Spreafico MC, Sternai P, Agliardi F (2020) Paraglacial rock-slope deformations: sudden or delayed response? Insights from an integrated numerical modelling approach. *Landslides*, 1–16
- Stead D, Wolter A (2015) A critical review of rock slope failure mechanisms: the importance of structural geology. *J Struct Geol* 74:1–23. <https://doi.org/10.1016/j.jsg.2015.02.002>
- Sternai P, Herman F, Champagnac JD, Fox M, Salcher B, Willett SD (2012) Pre-glacial topography of the European Alps. *Geology* 40:1067–1070
- Studio Cancelli Associato (2017) Studio “Modellazione geotecnica ed individuazione delle soglie di criticità nelle aree di frana monitorate dal CMG di ARPA del lotto 1: aree di Val Genasca e Gallivaggio (Comune di San Giacomo Filippo, SO) e Monte Lete (Comune di Sueglio, LC) - Area di Monte Leté
- Tofani V, Raspini F, Catani F, Casagli N (2014) Persistent scatterer interferometry (PSI) technique for landslide characterization and monitoring. *Landslide Sci a Safer Geoenvironment Vol 2 Methods Landslide Stud* 351–357. 10.1007/978-3-319-05050-8_55
- Wasowski J, Bovenga F (2014) Investigating landslides and unstable slopes with satellite multi temporal interferometry: current issues and future perspectives. *Eng Geol* 174:103–138
- Zanchi A, Crosta GB, Stelluti G, Sterlacchini S (2002) 3D geolocal modeling for slope stability problems. The case study on the Corno Zuccone sacking Val Taleggio (Italy). *Mem Soc Geol It* 57:585–594
- Zischinsky U (1966) On the deformation of high slopes. In: 1st ISRM Congress. International Society for Rock Mechanics and Rock Engineering

Supplementary Information

The online version contains supplementary material available at <https://doi.org/10.1007/s10346-021-01654-0>.

C. Crippa (✉) · **E. Valbuzzi** · **P. Frattini** · **G. B. Crosta** · **M. C. Spreafico** · **F. Agliardi**

Department of Earth and Environmental Science,
University of Milano-Bicocca,
Piazza della Scienza 4, -20126, Milano, Italy
Email: c.crippa16@campus.unimib.it